THE UNIVERSITY OF OKLAHOMA

GRADUATE COLLEGE

EXAMINING THE MICROSTRUCTURE, AGGREGATION, AND VISCOELASTIC GELLING BEHAVIOR OF MUCIN SOLUTIONS

A THESIS

SUBMITTED TO THE GRADUATE FACULTY

in partial fulfillment of the requirements for the

Degree of

MASTER OF SCIENCE

By

AUSTIN CURNUTT

Norman, Oklahoma

2019

EXAMINING THE MICROSTRUCTURE, AGGREGATION, AND VISCOELASTIC GELLING BEHAVIOR OF MUCIN SOLUTIONS

A THESIS APPROVED FOR THE

SCHOOL OF BIOLOGICAL, CHEMICAL AND MATERIALS ENGINEERING

BY

Dr. Keisha B. Walters, Chair

Dr. Sepideh Razavi

Dr. Jeffrey Harwell

Table of Contents

Acknowledgements

Thank you to Dr. Keisha Walters for patience, support, constant help, but mostly patience, during some of the most difficult years of my life. Thank you for believing in me two and half years ago when I talked to you about my interests, for pushing me when I needed it, and for working incredibly hard to make sure final deadlines were met.

Thank you to the other graduate students in the Polymer and Surface Engineering Laboratories (PolySEL): Collin Britten – for constant patience and willingness to help with anything no matter how busy he was; Brandon Abbott – for supporting silica nanoparticle synthesis, characterization and preparation, SEM micrographs, and time spent talking and listening; and Kayla Foley – for being a gracious officemate and always offering water or extra snacks.

Thank you to Kaylee Smith, a former undergraduate at OU for help with literature searching, report writing, experimental design, sample preparation, characterization, synthesizing silica nanoparticles, and initial data analysis. Thank you to Emily Darrow, another former undergraduate at OU, for help with sample preparation and rheology characterization.

Thank you to my committee members, Dr. Sepideh Razavi and Dr. Jeffrey Harwell, for their flexibility and commitment to supporting my work.

Thank you to Barbara Semar and Greg Kamykowski from TA Instruments for help with rheology as well as Paul Simitis from Dataphysics for help with surface tension data.

Thank you to my family, for being understanding during stressful times and doing their best to support me throughout my education.

Last of all, thank you to Bridgitte Castorino, who was always there for me, even when her own life was busy and stressful. Thank you for being with me in times of peace, joy, frustration, and despair, for learning how to better support me and loving me through it all.

Abstract

Mucin solutions offer a simplified, yet still very complex, opportunity to study the microstructural and mechanical properties of mucosal fluids. The complex viscoelastic behavior of mucus is a result of electrostatic and hydrophobic interactions of large, polymeric mucin glycoproteins with other mucin molecules and their environment. Understanding mucin behavior and how to manipulate it is a crucial research field, presenting opportunities for advancement in drug delivery through mucosal membranes as well as mucus-related conditions like chronic obstructive pulmonary disease (COPD) and cystic fibrosis.

Work presented here is aimed at developing a stronger understanding of mucin microstructural and viscoelastic properties and the effects of pH, calcium chloride, small molecule compounds, and negatively-charged silica nanoparticles (SiNPs). Specifically, findings are presented regarding (1) the sol-gel transition behavior and the effect of pH and Ca^{2+}, (2) the effects of choline chloride, phenylboronic acid, and triethanolamine on mucin aggregation and rheology, and (3) synthesis of SiNPs and their effects on mucin aggregation and rheology. The data and findings presented were characterized using frequency-dependent rheology, dynamic light scattering (DLS) particle measurements, zeta potential (ZP), Fourier-transform infrared spectroscopy (FTIR), and Du Noüy ring surface tensiometry.

Mucus was simulated using solutions of porcine gastric mucin (PGM) in water and concentration was held constant throughout the entire study. pH modification and $CaCl_2$ addition were used to modify the gelling behavior of mucin, which was characterized *in situ* using all the methods described above. Small molecule compounds were obtained and added to mucin solutions to induce changes in mucin-mucin interactions, measured using DLS, ZP, and rheology. SiNPs were synthesized, characterized, and added to mucin solutions and their effects were also measured using DLS, ZP, and rheology.

The results demonstrate the known phenomenon of PGM aggregation and gelling at pH $\leq$4, as well as an increase in viscoelastic properties at pH 4.0 and 5.8 with the addition of $CaCl_2$ at 10 mM. FTIR was used in a new way to demonstrate increased glycosylation in mucin solutions at pH values of 2-5, suggesting a mechanism for aggregation seen through other methods. Rheological results for the small molecule compounds were mixed, but DLS and ZP confirmed a reduction in aggregation of ~70% at higher concentrations of each compound. The effects of ion content and changes in pH may have played a role, but do not interfere with or contradict the general finding. The Stöber process was successfully used to synthesis fairly uniform SiNPs, which produced consistent trends in PGM behavior. As negatively-charge particles with -OH functionality, they behaved similar to phenylboronic acid, inducing a decrease in viscoelastic properties at all concentrations and a decrease in ZP and particle size with increasing NP concentration.

Chapter 1. Introduction

1.1. Biological Role of Mucus and Implications for Health

On a daily basis, most people do not have regular thoughts about their mucus unless they are sick, deal with chronic allergies, or have a mucus-related condition like chronic obstructive pulmonary disease (COPD) or cystic fibrosis (CF). In fact, most people don't think about the majority of their bodily functions until something goes wrong. Most of the time, our bodies function well and keep us healthy, but they are constantly bombarded with external threats in the forms of bacteria, viruses, particulate matter, and harmful chemicals. There are also an endless variety of ways our health can be negatively impacted by internal factors like genetic predisposition to disease, a weak immune system, unbalanced gut microflora, or poor metabolism.

With the numerous internal and external threats to human health, it is quite incredible that the average person stays healthy for much of their life. Thousands of years of hominid evolution have resulted in a species that not only survives the numerous threats to our health, but actively searches out new ways to improve our health. Through advancements in basic sciences, physiology, pharmacology, medicine, and engineering, we have been able to mitigate and sometimes even eradicate diseases and dangerous health conditions.

Our bodies constantly work to protect us from threats, and one of the primary lines of defense in our bodies is something most of us rarely think about. Mucus is everywhere in our bodies. It is the interface between our body and the environment via our respiratory tract, mouth and eyes, digestive system, and reproductive tracts. It is a critical part of so many major biological functions including respiration, reproduction, and digestion, and it plays a role in the senses of sight, smell, and taste. Arguably its most important functions are providing a protective barrier for the body, lubricating epithelium surfaces, and transporting harmful molecules away from the epithelium. Mucus is also incredibly important to hydrating respiratory and ocular tracts and acts as a selectively permeable layer for diffusion of gas in the eye and and lung as well as nutrients in the GI tracts[1].

Understanding mucus structure and behavior as well as how to manipulate its properties is an important task in the fields of medicine and biomedical engineering. First, it is vital to understand how it relates to diseases like COPD and CF as well as certain cancers. These are situations in which mucus needs to be understood because something is not functioning properly related to mucus in the body. On the other hand, there are often times when something else is wrong in the body and a chemical therapeutic needs to be delivered.

Delivery of a therapeutic through the epithelium is very efficient, if the therapeutic can reach it quickly. Goblet cells imbedded in the epithelium exist to make sure this doesn't happen, secreting mucus which usually forms a two-phase layer along the epithelium (Fig. 1). The outer layer often exists in a gelled state characterized by aggregation of mucin, the structural biopolymer in mucus, viscous behavior, and reduced transport properties. The inner layer usually behaves more like a solution, with less mucin aggregation and better transport properties. The outer, gelled

layer works to adhere to and trap particles, while the inner layer serves to transport them away from the epithelium, protecting the body from a harmful particle or chemical.

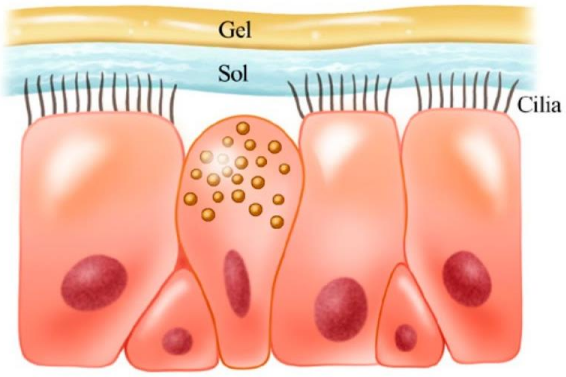

Figure 1. Goblet cells in epithelium secrete mucus to protect epithelium and transport safe particles through the solution regime. Reproduced from Yali Cadena[2].

When the particle or chemical is a therapeutic meant to treat a patient's disease or condition, the incredible protective and transport properties of mucus pose a problem. In these situations, it is vital to understand mucus structure and behavior so it can be modified to allow transmucosal delivery of a drug or treatment. A better understanding of these properties has and will continue to inform investigation and development of drug delivery vehicles that can penetrate mucus networks and deliver treatments efficiently.

1.2. Mucin and its Importance in Mucus Properties and Behavior

Mucin is a polymeric glycoprotein with complex polyelectrolytic behavior and is the main structual component in mucus. Mucus, which is 90-95% water, contains electrolytes (1%), lipids (1-2%), non mucin proteins (<1%), and mucin glycoproteins (1-5%), which themselves are 50-80% glycosylated carbohydrates by weight[1]. While mucus is mostly water, its microstructural and viscoelastic behaviors are largely due to the properties of mucin, making mucin a primary target for investigation into mucus-related applications, a general outline of which is provided in Fig. 2. Since the 1960s, mucus and mucin solutions have been a significant topic of research, of which many earlier studies focused on mucus-related conditions like cystic fibrosis[3–5]. Since then, research efforts regarding animal mucus and mucin have focused on understanding its composition[1,6–8], protective function[6,9–11], role in drug delivery[12–19], transport properties[10,20–23], and further examination of its role in COPD[24] and cystic fibrosis[21,25–27].

Mucin molecules are large and complex, meaning that study of mucin behavior can also be complex, requiring a large, continually growing body of work to understand it sufficiently. As mentioned, mucin proteins are made up of large glycosylated domains and smaller weakly or non-glycosylated domains. Large glycosylated domains form the center of mucin fibers, with monomer ends bound by von Willebrand Factor domains as well as cysteine knot and cysteine rich domains. Monomers are bound to each other through S-S disulfide bonding between the cysteine domains

and long chains are composed of alternating glycosylated and non-glycosylated domains, shown in Fig. 3. The mucin network structure is formed as a result of hydrophobic and electrostatic interactions between non-glycosylated domains in mucin multimers.

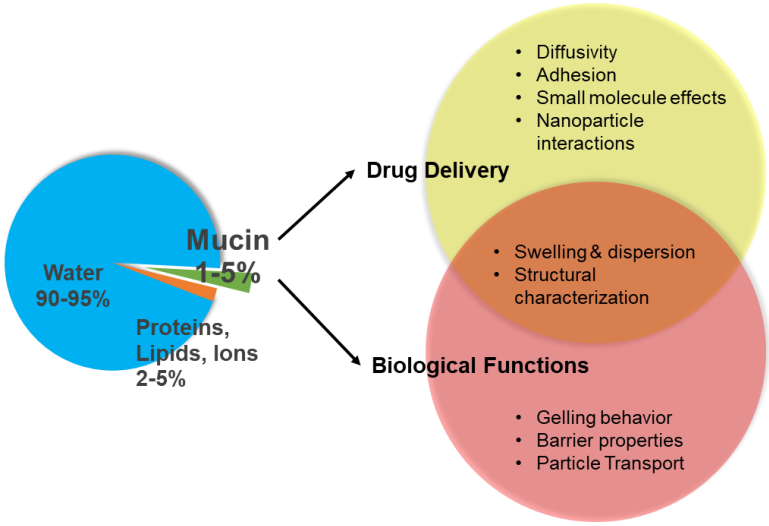

Figure 2. Mucus component breakdown and applications for the study of mucin.

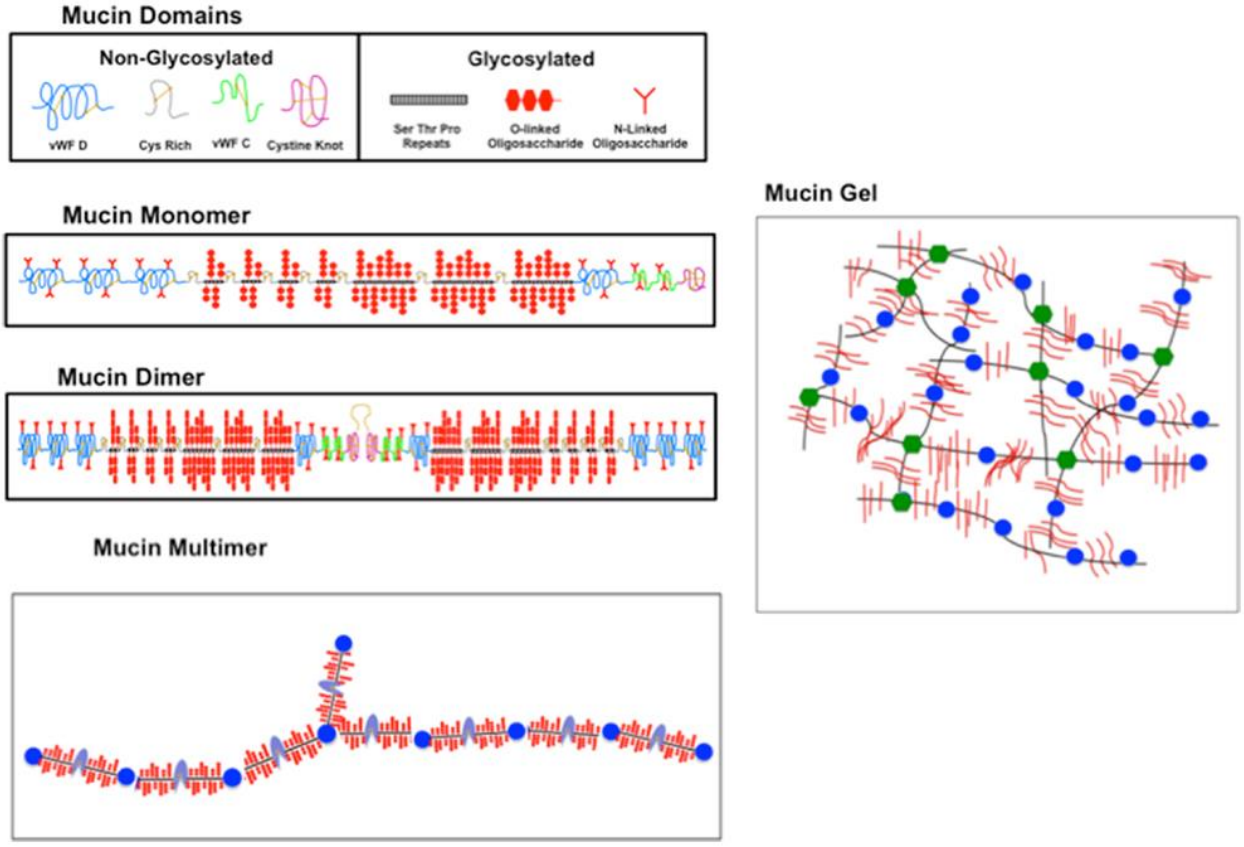

Figure 3. Mucin structure broken down by chemical domains. Reproduced from Bansil et al.[28]

While the structure is complex, it is known from previous work that mucin network formation is a result of hydrophobic[9,29,30] and electrostatic[9,31,32] interactions between mucin chains and disulfide bonding[33–35] between mucin monomers which drives mucin self-assembly. It is incredibly importatnt to continue the study of these interactions and develop new ways of manipulating them to control mucin behavior.

Mucin in solution behaves like a complex fluid, with variable properties that can be altered in response to environmental factors. The most well-known effects are seen with regard to the gelling behavior of mucus, which takes place at low pH values, generally less than 4[29,36–38]. When mucin is in the gel regime, it exhibits higher viscosity and decreased transport properties, which contribute to its ability to protect the body from foreign substances. Conversely, mucin solutions in the solution regime demonstrate behavior more closely resembling that of a liquid, with lower viscosity higher transport properties. This transition from solution to gelled behavior is known as the sol-gel transition and, in addition to pH, this can be manipulated through ion valency and concentration[32,38–40] as well as the addition of functionalized particles[7,24,41,42]. The potential for manipulation of mucin properties has provided a large opportunity for research and development of applied particles used to adhere to mucosal surfaces and penetrate them, both of these goals requiring a strong understanding of mucin chemistry and behavior.

1.3. Study Goals and Future Efforts

The purpose of the research presented in this body of work is to provide further understanding of the effects of pH, Ca^{2+}, various small molecular compounds, and nanoparticles on the chemical, microstructural, and mechanical properties of mucin solutions. To do this, partially purified porcine gastric mucin (PGM) solutions at 10 mg/mL were used as a model system to examine mucin behavior. A range of pH and $CaCl_2$ concentrations was evaluated in order to examine the sol-gel transition and how that transition can be manipulated. Mucin properties were examined using a variety of techniques including rheology, dynamic light scattering (DLS) particle sizing, zeta potential (ZP), Fourier-transform infrared spectroscopy (FTIR), and surface tension characterization. These efforts are presented with ion addition the focus of Ch. 2, small probe molecule addition in Ch. 3, and the addition of silica nanoparticles in Ch. 4. While findings and conclusions are given in each of Ch. 2-4, overall conclusions will be presented in Ch. 5.

Future efforts will include continued research into the interactions of various functional compounds with mucin and the resulting changes physicochemical, microstructural, and mechanical properties. These efforts will be focused on nanoparticle synthesis, functionalization, and testing and may include nanoparticles functionalized with polymers to promote mucoadhesion or mucopenetration. For drug delivery and therapeutic applications, particle surface chemistry and charge characteristics should be tailored towards producing desired changes in mucin properties to promote transport into mucosal membranes and increased adhesion once reaching a target. Amphiphilic compounds are promising for this application as their surface interaction can be controlled and regulated based on their chemical environment (pH, ion content, etc.).

The work presented here has flaws and inconsistencies that should also be addressed in future efforts. Most notably, rheological data was not always consistent with findings regarding

mucin particle size and surface charge. It may be useful to introduce micro-rheological techniques or particle tracking to understand what is happening to transport and viscoelastic properties on the micro-scale. With regard to data presented on small molecule effects, future work should do a better job of taking into account and reducing the effects of pH and ion content so that stronger conclusions can be drawn regarding the effect of each functional molecule.

Chapter 2. Characterization of Mucin Solution Gelling Behavior in Response to pH and [Ca^{2+}]

2.1. Abstract

In both the treatment of pathological conditions and drug delivery design, it is important to understand how the range of chemical states that may be present can affect mucus properties responsible for controlling transport and barrier function in biological systems. In this study, microstructural and viscoelastic properties of aqueous solutions of porcine gastric mucin (PGM)—the biopolymer in mucus—were investigated in response to changes in pH and $CaCl_2$ concentration. Mucin solutions were characterized using rheology, dynamic light scattering (DLS), zeta potential, surface tension, and FTIR spectroscopy to correlate microscale structural changes with macroscale viscoelastic behavior. A pH range of 2.1 to 5.8 was examined in PGM solutions, and a transition from solution-like to gel-like behavior occurred at and below pH values of ~ 4 which was accompanied by a more than 10x increase in viscoelastic moduli. Addition of 10 mM $CaCl_2$ increased the sol-gel transition pH value to nearly 5.8 and the mucin network structure demonstrated a doubling of the loss moduli at low frequencies and a 10x increase in the storage modulus. The addition of 10 mM $CaCl_2$ also caused an increase in the isoelectric point of PGM solutions and through increased glycosylation of PGM. The relationships demonstrated between pH and ionic effects on the sol-gel network transition in mucin can be extended to other biopolymers, biomimetic polymers and synthetic polyelectrolyte systems, as well as other hydrogel materials.

2.2. Introduction

Mucin is a polyelectrolyte glycoprotein found in mucus, the structured complex fluid found in all types of organisms from bacteria to humans. In vertebrates, mucus is produced by mucus membranes and can be found lining the eyelids, mouth, and nose, as well as gastrointestinal, respiratory, and genital tracts. Since the 1970s,[5] animal mucus and mucin solutions have been well studied, especially the roles mucus plays in drug delivery,[15,36,41,43,44] disorders like cystic fibrosis,[26,27] and its protective biological functions.[9,42,45,46] Mucin glycoproteins are present in mucus at concentrations of 1-5%, along with electrolytes (ca. 1%), lipids (1-2%), other proteins (1-2%) and water (90-95%).[47] Despite being present in low concentrations, mucin glycoproteins are primarily responsible for the protective and lubricative functions of mucus within the body.

Solubilized mucin behaves as a complex fluid with changing viscoelastic and structural properties in response to its environmental conditions. Mucin glycoproteins are responsible for the majority of the physical properties of mucus, and their conformation, intra- and inter-strand bonding and microstructure changes in response to environmental factors such as pH,[9,27,36,39] temperature,[15,48] and ion content.[5,39,40] All of these factors affect the reversible supramolecular bonding groups present in the protein strands, which modifies the microstructure as well as the mechanical and transport properties of the mucin network. Gel hydration also plays an important role in mucus properties,[25,49] as well as the size(s)[50,51] and surface chemistry[41,42,45,52–54] of any non-

native particles present. The ability for mucin solutions to reversibly form a gel is important for controlling the barrier properties of mucus and impacts not only disease protection and lubrication, but also drug delivery efficacy. The transition from solution state to gel state is accompanied by changes in interactions between mucin strands, physical structures present in solution, and mechanical properties. As shown in Fig. 4, the sol-gel transition in mucin solutions is reversible and the transition point can be modulated using parameters such as pH, temperature, and ionic strength.

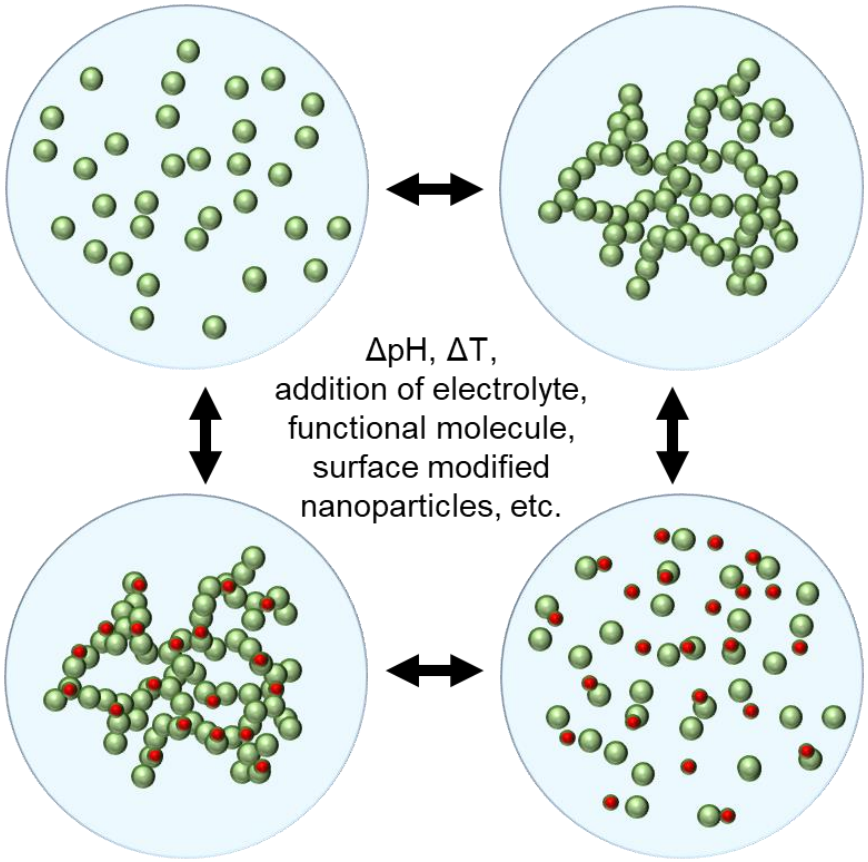

Figure 4. Sol-gel transitions can take place in structured fluids in response to changes in environmental factors such as pH, ion concentration, particle chemistry, temperature and/or shear forces. Gels form when the self-affinity of solubilized material increases while the aggregates remain soluble.

Native mucus, especially non-reconstituted, can be difficult to obtain without regular access to human or animal subjects, so porcine gastric mucin (PGM) solutions are often used a model for mucus studies. PGM solutions are generally considered a viable system to examine mucus sol-gel behavior due to the relative ease of extraction, availability, and biological function exhibited[9,38,55], although this point was debated by Crater et al. in a study on nanoparticle transport.[56] The main benefit of using PGM solutions is facilitation of fundamental studies of mucin behavior by removing variations in mucin concentration, type, and extraction method that can occur between different patient (native mucus) sources. By eliminating variability in the

mucin composition, interactions between mucin, effects of pH and salt on the sol-gel transition, rheology, and particle size distributions can be effectively studied.

An examination of the literature provides a number of studies that each examine isolated aspects of mucus and mucin properties, but these properties are often not connected, especially within the same body of work. The microstructure and mechanical properties of mucin have been characterized using rheology[36,57], light scattering techniques[29,48], zeta potential[58,59], infrared spectroscopy[58,60], and various other techniques. Of these methods, IR spectroscopy is the most recently used tool (as it was not used before 1995[38]) and shows promise for demonstrating glycosylation in mucin[61].

In order to gain a better understanding of the complex relationships between chemical and structural properties of mucin, these and other studies have been performed on mucus and various forms of mucin, although many focused on a single characterization technique or aspect of mucin property changes. This study is intended as an effort to characterize and more clearly correlate micro- and macro-scale properties of mucin during the sol-gel transition by examining the results of pH and ion effects over multiple length scales. Mucin viscoelastic behavior was examined using oscillatory frequency sweep and flow sweep rheology experiments, and the elastic and storage moduli and viscosity were measured as a function of pH and Ca^{2+} ion concentration. In addition to rheological characterization, structural properties related to mucin-mucin interaction and the sol-gel transition were studied using zeta potential, dynamic light scattering, surface tension, and Fourier transform infrared spectroscopy. Particle size and particle size distribution data were coupled with changes in net surface charge, interfacial tension, and functional group interactions to examine the how the microstructural changes observed with rheology could be correlated to molecular-level changes. Structure-property changes related to the sol-gel transition for PGM was examined with regards to ion effects and pH value. A better understanding of the relationship between the viscoelastic behavior of mucin and its dynamic network structure is critical for predicting and controlling mucin properties, which can aid in designing therapeutic treatments for diseases and drug delivery vehicles related to mucus.

2.3. Materials and Methods

Materials. Solutions of PGM mucin (Type II, Sigma Aldrich, CAS No. 84082-64-4) at 10 mg/mL were prepared using filtered Nanopure™ water. The concentration of PGM solutions was kept at a constant 10 mg/mL in accordance with another study[29], allowing observation of pH and ion effects on gelling behavior to be decoupled from the effects of higher concentration. For the rheology study, nitric acid and potassium hydroxide were used to form a series of PGM solutions at various pH values. Samples of PGM in water (neat) with an 'as prepared' pH value of 3.83 ± 0.03 were adjusted to three discrete pH values of 2.1, 4.0, and 5.8. In addition to these pH-adjusted PGM samples, a set of PGM solutions was prepared by adding 10 mM calcium chloride (via calcium chloride dihydrate, VWR International, ≥99%) to the aqueous PGM solutions at each pH value tested. PGM solutions were prepared over a wider pH range—at values of 2.1, 3.0, 4.0 and 5.0—in the same manner as described previously to test the impact of pH and calcium chloride concentration using zeta potential (ZP), dynamic light scattering (DLS) particle sizing, and FT-IR

spectroscopy characterization methods. All solutions were stirred vigorously over a period of 4-8 hours and refrigerated overnight to obtain homogeneous solutions prior to characterization and allowed to warm to room temperature for characterization. (Solutions were also refrigerated between sampling events.) To obtain zeta potential and particle sizing data, the 10 mg/mL PGM solutions were stirred 4-8 hours until homogeneous and then were diluted 100x to 0.1 mg/mL for the light scattering experiments.

Rheology. Rheological measurements were collected with a TA Instruments Discovery Hybrid Rheometer II (DHR-2) using TRIOS software (v4.3). A 40 mm cone and plate geometry with 2.013° angle and a 53 μm gap was used for frequency and flow sweeps. The cone and plate geometry was chosen to maintain a constant shear rate throughout each sampling period. Rheological data were obtained using a solvent trap to discourage evaporation during each run and maintain proper filling of the sample liquid.

Frequency and flow sweeps were performed on 6 samples at 3 different pH values both with and without the addition of $CaCl_2$. PGM concentration and temperature were also examined in a more cursory manner. Higher concentrations (20-60 mg/mL) were shown to increase viscoelastic properties, but increasing temperature to a more physiologically relevant 37 °C had almost no effect on these values (see Appendix).

To perform frequency sweeps, the linear viscoelastic regime (LVR) of each sample was determined to ensure that the measure properties are independent of imposed strain. Tests performed in this region are reliable and more reproducible.[62] The LVR is the range of shear stress values over which the elastic modulus (G') and the loss modulus (G'') and other viscoelastic properties are independent of applied forces.[63] Frequency sweeps were performed in the LVR to ensure the mucin properties are independent of strain, allowing the viscoelastic moduli to be assessed consistently between samples. To determine the LVR, an oscillating amplitude sweep was performed on each sample at a frequency of 1 rad/s over a stress range of 0.01 to 100 Pa. The LVR was determined by choosing the average strain value that produces constant elastic moduli values (in the range of ~0.01 strain for each sample). Frequency sweeps were performed at each sample's strain value related to the LVR at 25 °C over a 0.01 to 100 rad/s frequency range. All error values for data are displayed or written as 95% confidence intervals.

Flow sweeps were performed on a range of shear rates from 0.001 to 100 s^{-1} at 25 °C with a sample period of 30 s for each data point collected. All error values for data are displayed or written as 95% confidence intervals.

Zeta Potential. A Brookhaven Instruments Nanobrook Omni phase analysis light scattering (PALS) instrument was used to perform zeta potential experiments. To obtain zeta potential data as a function of pH a BI-ZTU 4-pump autotitrator unit was utilized along with a BI-ZELF flow cell. The PALS program within the Brookhaven Instruments Particle solutions software was used to control experiments and collect and analyze data. The flow cell was rinsed with Nanopure™ water and emptied before each experiment. The pH of the sample was modified by the autotitrator with nitric acid and potassium hydroxide, and then zeta potential measurements were collected at each discrete pH value in order to determine the pH value for the point of zero charge (pzc).

Dynamic Light Scattering Particle Sizing. The Nanobrook Omni PALS instrument equipped with Brookhaven Instruments Particle Solutions Software was also used to perform particle sizing via dynamic light scattering (DLS). DLS measurements were collected for the PGM solutions at discrete pH values of 2.1, 3.0, 4.0, and 5.0.

Surface Tension. A Dynamic Contact Angle Measuring Device and Tensiometer (DCAT) 25 from Dataphysics was used to measure the surface tension of PGM solutions at discrete pH values of 2.0, 3.9, and 6.0. All measurements were taken using a Du Noüy ring geometry and data analyzed using DCATS software and Microsoft Excel.

FT-IR. FT-IR spectroscopy experiments were performed using a nitrogen-purged Thermo Fisher Nicolet iS50 instrument using a deuterated triglycine sulfate (DTGS) detector, attenuated total reflectance (ATR) accessory with diamond-ZnSe crystal and a XT-KBr beamsplitter. PGM solutions were each deposited dropwise onto the ATR crystal and spectra collected (with a minimum of 256 scans) using ambient air as background. Absorbance spectra were collected and analyzed using Thermo Scientific OMNIC™ software. Water spectra were collected and subtracted from each sample spectra to remove absorbance bands from the sample solvent.

2.4. Results and Discussion

Electrostatic and hydrophobic interactions have a significant impact on protein conformation, solvency, interactions with substrates and particulates and barrier properties.[1,38,64] The ionic state of the solution can be adjusted by changing the pH, ionic strength and ion valencies present.[1,9,43] By adjusting the solution ionic state, sol-gel transitions can be controlled in mucus and mucin solutions[1,5,32]. Calcium chloride was added to mucin solutions as multivalent cations have been shown to impact mucin conformation even at very low concentrations (~1 mM).[4,5,32] Unlike the electrostatic screening seen in monovalent ion studies, the multivalent ions show evidence of binding with specific anionic sites on mucin side chains. In addition, calcium (Ca^{2+}) is known to play a role in cystic fibrosis, where increased concentration is known to increase density and viscosity and decrease solubility of mucus.[4,27]

Fig. 5 shows the results of six independent measures run at 25 °C from 0.01 to 100 s^{-1} shear rate on 10 mg/mL PGM solutions at various pH values with and without 10 mM $CaCl_2$ (denoted by PGM+Ca^{2+}) The results illustrate non-Newtonian shear-thinning behavior in mucin solutions; these higher shear rates studied correspond to physiological processes like inhalation and coughing.[65,66] As shown in Fig. 5, the addition of a small concentration of calcium results in a significant increase in viscosity. This is a significant finding as calcium is known to play a strong role in not only mucus secretion but also the intragranular storage of mucin.[67] A better understanding of the rheological behavior of mucus and mucin solutions under physiological conditions is important for designing pulmonary therapeutics and drug delivery applications.

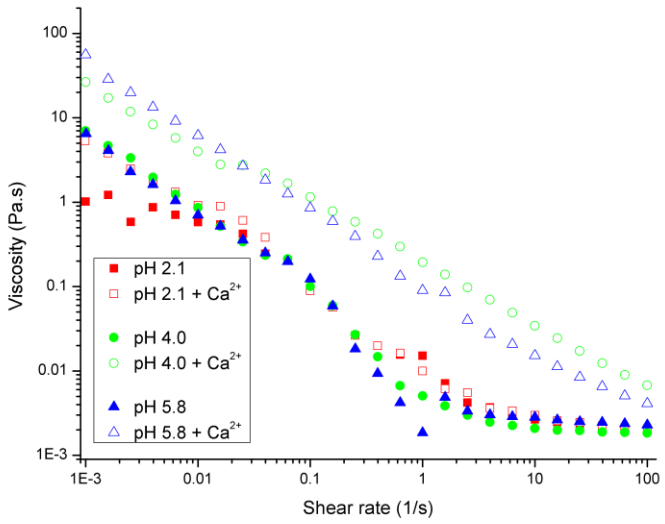

Figure 5. Flow sweeps over a shear rate of 0.001-100 s^{-1} show samples at pH 2.1, 4.0, and 5.8 with 10 mM $CaCl_2$ display shear-thinning behavior.

To further understand the structural responses of mucin, oscillatory sweeps over a low frequency range were performed to characterize PGM gelling behavior. Fig. 6 shows the results of the average of three frequency sweeps performed on PGM solutions at pH 2.1, 4.0, and 5.8. There is a clear response due to changes in pH, shown by the transition from gel-like behavior at pH 4 and below to liquid-like behavior in the sample at pH 5.8. This response matches previous work done with PGM solutions, indicating a transition to gel behavior taking place at pH 4 and below.[36]

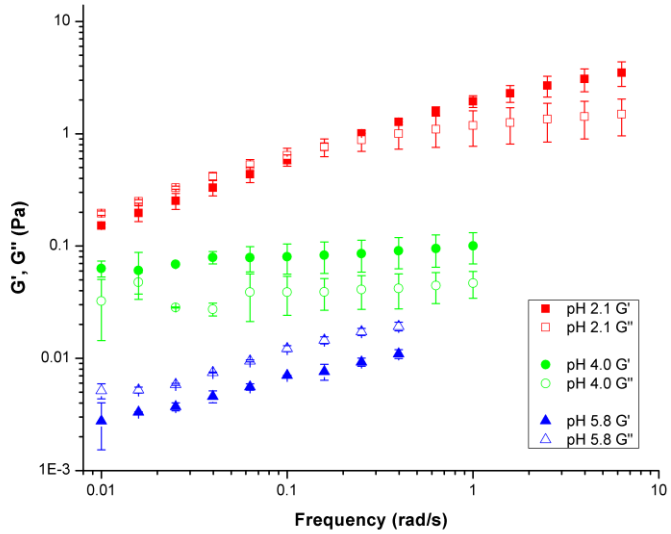

Figure 6. Oscillating frequency sweep rheology data over 0.01-100 rad/s for aqueous PGM solutions showing G' (closed symbols) and G'' (open symbols) at pH values of 2.1, 4.0, and 5.8.

Fig. 7 shows the results of the same experiments performed on PGM solutions at pH 2.1, 4.0, and 5.8 with added $CaCl_2$ at 10 mM. As discussed previously, the sol-gel transition takes place around pH 4 for neat PGM solutions and the frequency sweep data in Fig. 7 shows the effect of Ca^{2+} on either side of the pH-induced sol-gel transition. With the addition of calcium chloride, the moduli of the pH 2.1, 4.0, and 5.8 samples respectively decreased, increased, and increased. Below pH 4, the addition of calcium chloride caused a decrease in viscoelastic moduli, likely indicating a disruption of the mucin polymeric structure. At pH 4.0 and 5.8, the opposite was true which potentially indicates a stabilizing mechanism in which the mucin particles were able to bind more strongly with one another. The samples at pH 4.0 and pH 5.8 both showed an increase in G' and G'' with the addition of calcium chloride. However, the pH 5.8 sample showed a transition from solution to gel-like behavior, again indicative of a stabilizing mechanism. It is possible that the pH 4.0 sample was just entering the gel regime and displayed behavior indicative of both regimes.

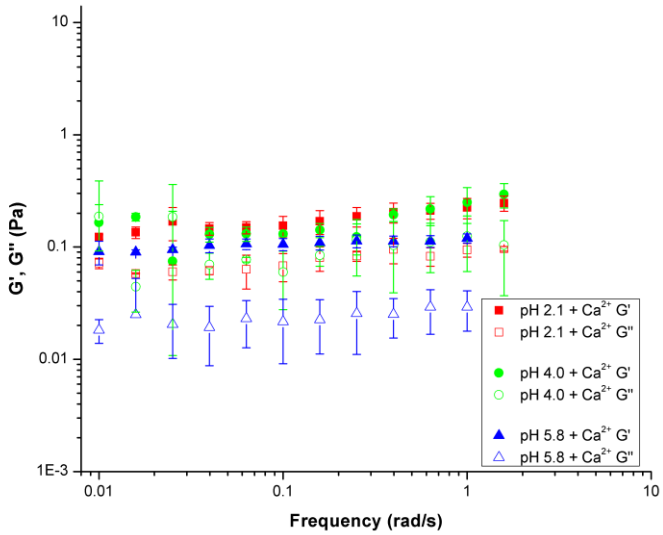

Figure 7. Oscillating frequency sweep rheology data over 0.01-100 rad/s for aqueous PGM solutions at pH values of 2.1 (triangle), 4.1 (square), and 5.8 (circle), with 0.01M calcium chloride added.

The PGM mucin solutions at pH 2.1 are in the gelled regime (Fig. 8), as exhibited by the dominant elastic moduli in both samples. In this regime, the addition of 10 mM calcium chloride caused a decrease in both the elastic and storage moduli. Divalent ions, such as calcium, are known to cause the mucin gel to collapse at low pH because of the fixed nature of the mucin's negative charges.[68] This behavior is exhibited in the PGM samples, where it is clear that the presence of Ca^{2+} caused a decrease in viscoelastic properties. It should be noted that the elastic modulus continues to dominate the sample viscosity, indicating gel behavior even with $CaCl_2$ present.

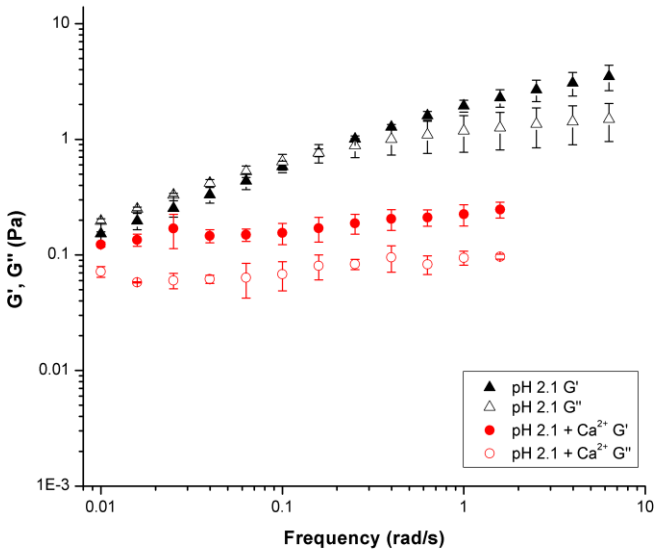

Figure 8. Storage (G') and loss (G") moduli of PGM solutions at pH 2.1 are shown to decrease with the addition of 10 mM calcium chloride.

The solutions at pH 4.0 (Fig. 6) are also in the gelled regime, as seen by the dominant elastic moduli. However, in this case, both the elastic and storage moduli of the samples increase with the addition of 10 mM calcium chloride. This behavior suggests that the addition of $CaCl_2$ may promote intramolecular bonding between PGM fibers.

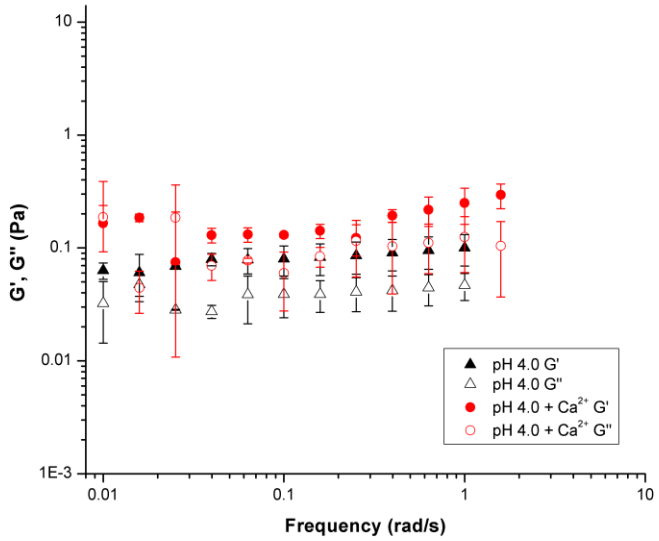

Figure 9. Storage (G') and loss (G") moduli of PGM solutions at pH 4.0 increase with the addition of 10 mM calcium chloride.

Examining Fig. 10, the PGM solution at pH 5.8 shows solution-like behavior in the absence of calcium chloride, as indicated by the loss modulus dominating the elastic modulus. With the addition of calcium chloride, the pH 5.8 PGM sample—like the pH 4 solution—showed an increase in both moduli. However, unlike the pH 4.0 PGM samples, pH 5.8 PGM exhibited a transition to the gel regime upon addition of $CaCl_2$, as shown by the dominant elastic modulus.

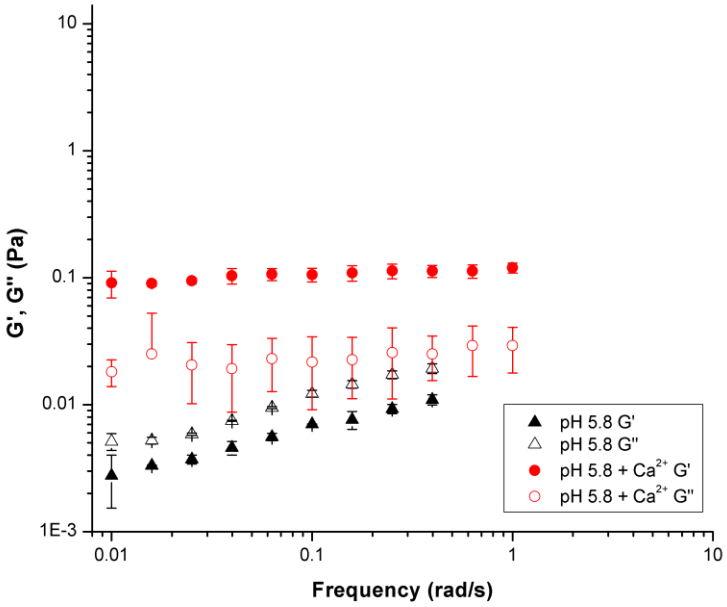

Figure 10. Storage (G') and loss (G'') moduli of PGM solutions at pH 5.8 increase with the addition of 10 mM calcium chlorides.

At higher, more neutral pH values (~5-7), PGM molecules are largely electronegative. Their non-glycosylated domains are arranged with salt bridges between carboxylates and positively charged amino acids (pKa values around 4) enfolded around the hydrophobic regions of PGM[9]. In this neutral pH regime, the addition of Ca^{2+}, a positively charged divalent ion, can disrupt the salt bridges, exposing the hydrophobic domains and promoting aggregation of PGM molecules through crosslinking, illustrated in Fig. 11. This is supported by previous work by Raynal et al. which demonstrated a significant increase in the molecular weight and viscosity of salivary mucin in the presence of 10 mM $CaCl_2$[69]. At lower pH values (≤4), aggregation is promoted through the side chain interactions, which result in folding of mucin strands and intermolecular crosslinking to take place. In this low pH regime, Ca^{2+} may play a different role, maintaining the gelled behavior of mucin but causing swelling as it substitutes for H^+ ions.

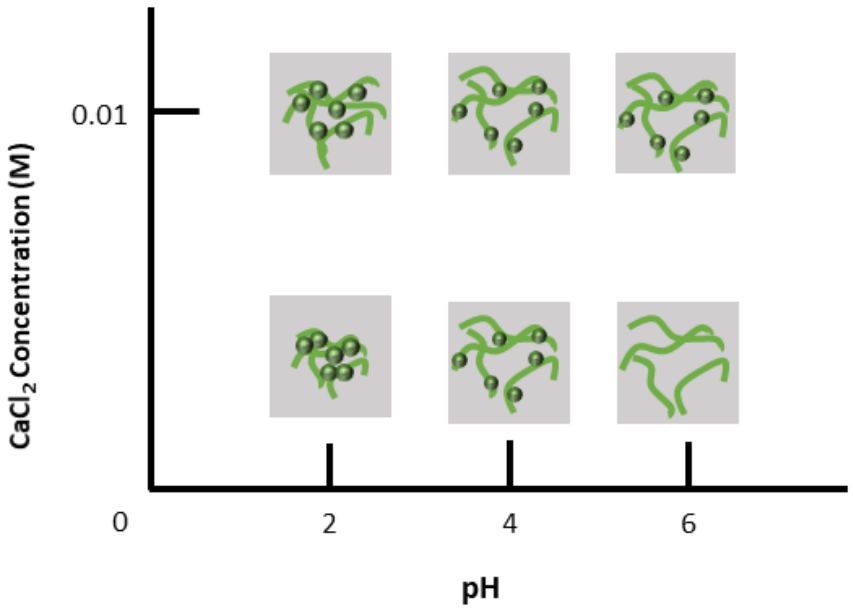

Figure 11. Visualization of PGM structural changes proposed from the rheological behavior as a function of pH and $CaCl_2$ concentration. At pH 2, addition of $CaCl_2$ induces slight swelling, at pH 4, almost no effect, and at pH 5.8, a transition from solution- to gel-like behavior.

Both electrostatic and hydrophobic interactions of the mucin dictate gelling behavior. Therefore, the effect of pH and $CaCl_2$ addition was examined for PGM solutions using zeta potential-a method to measure net surface charge of materials in dilute solutions. PGM particles in aqueous solution typically have a negative surface charge at pH values of 3 and above [58,70], so zeta potential measurements were taken at discrete pH values ≤ 4 to examine the effects of $CaCl_2$. Zeta potential as a function of pH are displayed in Fig. 12. Comparing the results of the neat PGM solution to PGM+Ca^{2+} revealed that the addition of $CaCl_2$ increased the isoelectric point (pI) of PGM particles. This increase in pI implies that electrostatic forces are neutralized at a higher pH value with the addition of $CaCl_2$, which correlates with the increase in viscoelastic properties seen in the rheological experiments. The addition of $CaCl_2$ shifted the isoelectric point, where the zeta potential is 0 mV, from ca. pH 2.75 to pH 3.1. This finding is a result of the ability of added Ca^{2+} ions to expose hydrophobic domains in mucin and neutralize the negative surface charge of PGM. At low pH values, the impact of the Ca^{2+} ions is mitigated, as there is a large concentration of H^+ ions available in solution.

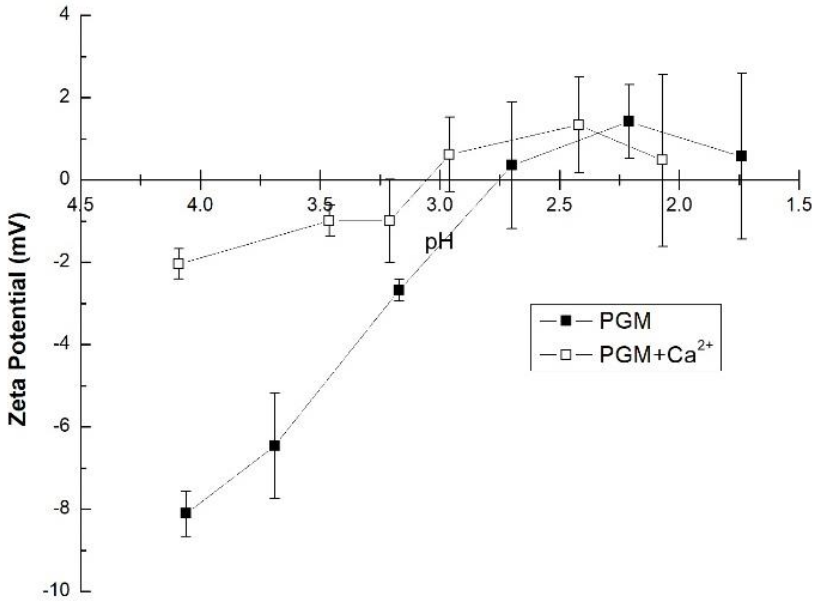

Figure 12. Zeta potential data show a higher isoelectric point for PGM solutions with 10 mM $CaCl_2$ present.

Mucin solutions form large, non-uniform polymeric particles. The state of the mucin structure in solutions can be analyzed using dynamic light scattering (DLS) to determine average particle sizes and particle size distributions in solution. The average hydrodynamic particle size and particle size distributions measured using DLS were compared for PGM solutions with and without $CaCl_2$ added and at varying pH levels. The DLS data was analyzed to determine the dominant peak, in terms of number of particles present, in order to determine a metric of 'average' particle size for each sample. The average particle diameter by number data display a clear and sharp increase in particle size at pH values ≤ 4 (Fig. 13). Results from studies by other researchers[29,31,36], as well as data from this study, show that PGM undergoes a sol-gel transition around pH 4. The particle size data in Fig. 13 clearly illustrate the structural changes associated with the sol-gel transitions—as the average diameter increases approximately 5-fold at pH values of 4 and below. This increase in effective particle size is the result of increased interactions between adjacent PGM strands/particles. These mucin-mucin interactions are due to multiple supramolecular interactions including hydrophobic and electrostatic interactions[29,37], disulfide linkages[33,34], and glycosylation[10], which is known to increase in highly acidic environments[71].

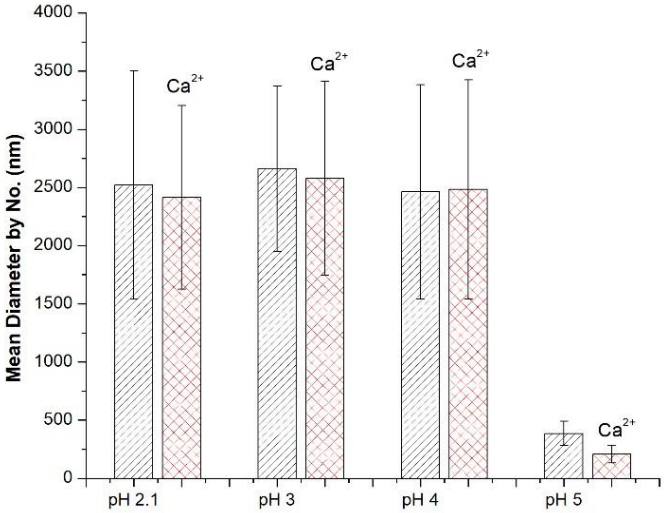

Figure 13. Average PGM hydrodynamic diameters determined by DLS reveal a sharp decrease in effective particle size at pH 4 and above, regardless of $CaCl_2$ addition of 10 mM.

Fig. 14 presents the results of surface tension measurements taken for PGM solutions at pH 2.0 (n=4), pH 3.9 (n=4), and pH 6.0 (n=3). The results show a clear decrease in surface tension corresponding to the solution regime as a function of pH. This supports the DLS particle sizing data that showed a decrease in particle aggregation above pH 4. In addition to this finding, the Du Noüy ring method also induced a shear-thinning effect in which the surface tension decreased as a function of each pull and push of the geometry in the solution (see Appendix).

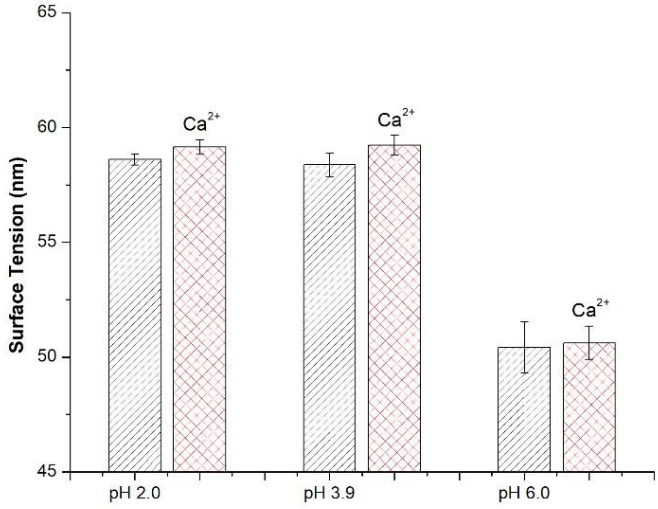

Figure 14. PGM solutions show a clear decrease in surface tension at pH values corresponding to the solution regime. Addition of 10 mM $CaCl_2$ had a negligible effect on the surface tension.

FT-IR analysis (Fig. 15) was used to identify functional groups present in the neat and pH-adjusted mucin samples, as well as changes in absorbance upon the addition of calcium chloride. Samples showed absorbance peaks in the range of 3200-3300 cm^{-1} which likely indicate O-H stretching of a carboxylic acid, but this was especially pronounced in samples with added $CaCl_2$. In fact, across all wavenumbers, absorbance was around fourfold higher in samples with $CaCl_2$. Shoulders indicating C-H stretching were also seen in the samples with $CaCl_2$ (~2950-2800 cm^{-1}) as well as strong peaks at 800 cm^{-1} and below which may be N-H out of plane bending or C-Cl stretching. All samples had C=C stretching between 1640 and 1620 cm^{-1} with larger differences found at lower wavenumbers. Strong C-O stretching peaks at 1260, 1095, and 1020 cm^{-1} (carbohydrate region) in samples with added $CaCl_2$, with the most pronounced found in the pH 2 solution with $CaCl_2$. This indicates stronger C-O bonding and glycosylation of mucin proteins, which strengthen polymer-polymer interactions within the mucin network.[61] This increase in absorbance and the indication of glycosylation provides evidence for increased intramolecular bonds as a result of Ca^{2+} interactions with the PGM network. Disulfide bonding, although known to play a role in this process, is much more difficult to characterize using spectroscopy and was not seen here[72].

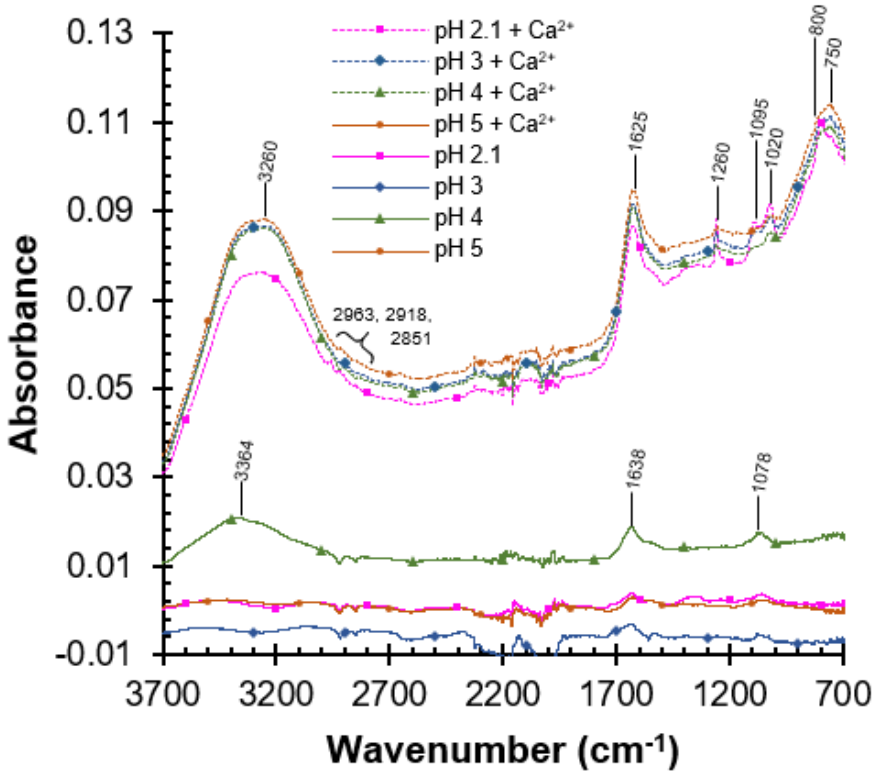

Figure 15. Representative FTIR spectra of 10 mg/mL PGM solutions at various pH values, both with and without 10 mM $CaCl_2$.

2.5. Conclusions

Solutions of porcine gastric mucin (PGM) were shown to exhibit a sol-gel transition that could be shifted using pH and addition of divalent $CaCl_2$. Rheological behavior of PGM solutions was shown to be highly sensitive to shear forces. All solutions exhibited shear-thinning behavior in flow sweeps, which showed an increase in viscosity for solutions at pH 4.0 and 5.8 with the addition of $CaCl_2$. PGM solutions without $CaCl_2$ exhibited gel-like behavior at pH values at and below ca. pH 4. With the addition of $CaCl_2$, viscoelastic moduli decreased at pH 2.1 and increased at pH 4.0 and 5.8, which matches the increase in viscosity shown from flow sweep experiment. The addition of $CaCl_2$ also induced a transition to gel-like behavior at pH 5.8, illustrating an increase in the sol-gel transition point. Zeta potential measurements supported the well-known gelling behavior of PGM at low pH values (<4) and illustrated the stabilizing effect of $CaCl_2$. Zeta potential of PGM solutions was around 0 mV below ca. pH 3 and a slight increase in isoelectric point of PGM was seen with the addition of $CaCl_2$ due to the neutralization of negative mucin surface charges by Ca^{2+} ions. Particle sizing results showed an approximately five-fold increase in effective particle size for mucin solutions at or below pH 4.0. The larger effective particle size as a result of aggregation supports a gelled mucin network existing in more acidic conditions. These data were supported by surface tension measurements, which also showed increased values at and below pH 4.0. In addition to these findings, FTIR spectroscopy illustrated a portion of the chemical nature of the stabilizing effect of $CaCl_2$, which promotes intramolecular bonding via glycosylation in mucin aggregates. Future work will focus on characterizing the effects of various chemistries and molecule types on the structural and mechanical properties of mucin solutions.

Chapter 3. Using Small Molecules to Chemically Disrupt Mucin-Mucin Interactions

3.1. Abstract

Electrostatic effects are known to drive the structural properties of porcine gastric mucin (PGM) and can be regulated through the addition of functional compounds. Choline chloride (ChCl), phenylboronic acid (PBA), and triethanolamine (TEA) were used as model compounds to investigate the effects of quaternary ammonium, alcohol, and tertiary amine groups to alter mucin structure and viscoelastic properties. ChCl induced up to a 100-fold increase in viscoelastic behavior, caused an approximate 70% decrease in particle size, and maintained a constant zeta potential at all concentrations, which suggesting more investigation into that compound. PBA and TEA showed mixed results of increased viscoelastic behavior at only 0.01 M, which was coupled with a similar 70% decrease in particle size and a strong reduction in PGM zeta potential from -6.3 ± 0.30 mV to -13.31 ± 0.53 mV with PBA and -27.39 ± 0.95 mV with TEA, indicating significant dispersion of PGM particles. In the case of TEA, an increase in pH also played a role in the dispersion, but the decrease in particle size was also seen at pH values closer to that of PGM solutions in water (~3.83).

3.2. Introduction

While mucin is a minor component of mucus in terms of weight percent, it is the primary component in determining the microstructure and related properties, thereby controlling the biological functions to control transport and lubricate respiratory, genital, and digestive tracts[9]. It is also present in saliva, nasal passages, and eyelids, where it plays an important role as a first line of defense against bacteria, viruses, particulates, and chemicals harmful to the human body. Mucin, which comes both secreted and membrane bound forms[1], is a structured glycoprotein and is responsible for mucus's ability to adhere to, trap, and transport particles out of mucus membranes. Mucin's properties vary significantly depending on water content (hydration), but they are also dependent on pH[9,31,36,73], ion content[4,5,40], and the chemistry of trapped or diffusing particles[21,23,24,52,74]. The surface chemistry[24,75,76] and charge[19,21,23] play a large role in mucoadhesion and mucopenetration which are dependent on changes in the microstructure of mucin networks. These concepts are important to consider when developing treatments for mucus-related diseases like COPD and cystic fibrosis (CF) as well as applications for drug delivery through mucus membranes[19,41,77,78].

Work has been done by other researchers examining various combinations of mucus and nanoparticle systems functionalized with various surface chemistries[23,74,75,79–83]. To understand mucus and mucus-related biological systems more fully, it is useful to study the effect of the surface chemistry in a more direct way and decouple its effects from the size or shape of the polymer or nanoparticle solid substrates. The present study evaluates the effect of three small molecules, with each including different combination of functional group type and number, to examine the impact on changing the mucin properties. The hypothesis is that by adding these

small molecules, the bonding that occurs between mucin strands can be disrupted and change the microstructure. These changes in network microstructure will be evaluated using rheology, dynamic light scattering, zeta potential, and FTIR. Triethanolamine, a tertiary amine, choline chloride, a quaternary amine, and phenylboronic acid, an anionic alcohol, were chosen as the small interrogation molecules in this study. Amine-functionalized[49,56,84] and phenylboronic-functionalized[16,85,86,86] polymers and nanoparticles have been the subject of recent studies focused on mucoadhesion and drug delivery. The alcohol was chosen in order to provide similar chemistry to the silica nanoparticle study (Ch. 4).

3.3. Materials and Methods

Materials. Solutions of porcine gastric mucin (PGM, Type II, Sigma Aldrich, CAS No. 84082-64-4) at 1.0 w/w% (10 mg/mL) were prepared using filtered Nanopure™ water. Choline chloride (ChCl), phenylboronic acid (PBA, also known as benzeneboronic acid), and triethanolamine (TEA) were all received from ThermoFisher Scientific Chemicals (98+%, used as received) were added to 10 mg/mL PGM solutions at various concentrations (Table 1). Neat PGM solutions at 10 mg/mL in water, with no added molecules, have a natural pH value of 3.83 ± 0.03, which was not changed significantly in these samples, except those with TEA concentrations above 1 mM because it is a relatively strong base. All small molecule-doped PGM solutions were stirred vigorously and then refrigerated overnight to obtain homogeneous solutions. Prior to characterization the solutions were allowed to warm to room temperature (ca. 25 °C).

The compounds chosen for this study (chemical structures shown in Fig. 16) were selected because of their unique charge characteristics and potential ability to interact with and disrupt charged domains and side chains in PGM molecules. Choline chloride is a bifunctional molecule with both a quaternary ammonium salt and alcohol moiety, giving it potential amphiphilic properties. In solution, ChCl is highly electronegative with a surface charge of -37.08±0.74 mV. Phenylboronic acid is also very electronegative with a surface charge of -24.03±3.92 mV and pKa of 8.9[87]. It also behaves as a mild Lewis acid, allowing it to act as an electron acceptor. Triethanolamine is both a tertiary amine and triol with a surface charge of -7.06±1.81 mV and pKa of 7.76[88]. ChCl, PBA, and TEA have respective hydrogen bond donor and acceptor counts of 1 and 2 (ChCl)[89], 2 and 2 (PBA)[90], and 3 and 4 (TEA)[91], giving TEA the highest potential for electrostatic interactions with mucin domains. ChCl and TEA are both fully miscible in water[92,93] and while PBA has a predicted solubility limit of 10 mg/mL[94], the 0.1 M solution (12.19 mg/mL) was fully dissolved with no precipitation.

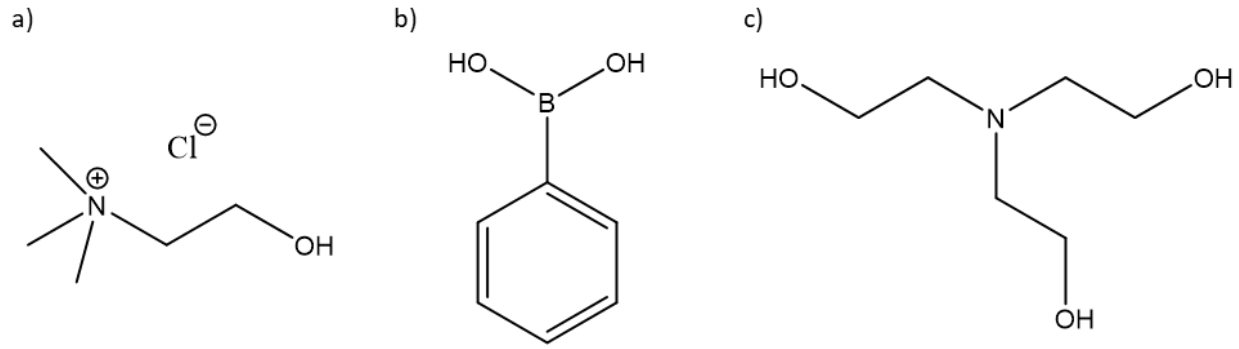

Figure 16. Chemical structures of a) choline chloride (ChCl), b) phenylboronic acid (PBA), and c) triethanolamine (TEA).

Table 1. Properties of PGM solutions at 10 mg/mL.

Choline Chloride (ChCl) + PGM			Phenylboronic Acid (PBA) + PGM			Triethanolamine (TEA) + PGM		
Sample	Conc. (M)	pH	Sample	Conc. (M)	pH	Sample	Conc. (M)	pH
C1	1.00E-05	3.817	P1	1.02E-05	3.812	T1	1.00E-05	3.802
C2	1.00E-04	3.812	P2	1.02E-04	3.807	T2	1.00E-04	3.818
C3	5.00E-04	3.804	P3	5.21E-04	3.807	T3	5.00E-04	3.894
C4	1.00E-03	3.794	P4	1.04E-03	3.806	T4	1.00E-03	4.003
C5	2.00E-03	3.789	P5	2.04E-03	3.803	T5	2.00E-03	4.228
C6	1.00E-02	3.785	P6	1.00E-02	3.808	T5	1.00E-02	7.099
C7	1.00E-01	3.731	P7	1.00E-01	3.773	T7	1.00E-01	8.652

Rheology. Rheological measurements were collected with a TA Instruments Discovery Hybrid Rheometer II (DHR-2) using TRIOS software (v4.3). A 40 mm cone and plate geometry with 2.013° angle and a 53 µm gap was used for frequency and sweeps. Rheological data were obtained using a solvent trap to discourage evaporation during each run and maintain proper filling of the sample liquid.

Frequency sweeps were performed on twelve samples at various concentrations of ChCl, PBA, and TEA (4 per molecule). To properly perform the frequency sweep measurements, first the linear viscoelastic regime (LVR) of each sample was determined to ensure that the measured properties are independent of the imposed strain. All frequency sweep experiments were performed in the LVR to ensure the mucin properties are independent of strain, allowing the viscoelastic moduli to be compared between samples. To determine the LVR, an oscillating amplitude sweep was performed on each sample at a frequency of 1 rad/s over a stress range of 0.01 to 100 Pa. The LVR was determined by choosing the average strain value that produces

constant elastic moduli values (on the order of ~0.01 strain for each sample). Frequency sweeps were performed at each sample's strain value related to the LVR at 25 °C over a 0.01 to 100 rad/s frequency range. All error values for data are displayed or written as 95% confidence intervals.

Zeta Potential. A Brookhaven Instruments Nanobrook Omni phase analysis light scattering (PALS) instrument was used to perform zeta potential experiments on each solution. The PALS program within the Brookhaven Instruments Particle solutions software was used to control the instrument during the experiments, as well as collect and analyze data. Zeta potential measurements were collected at each discrete concentration to assess the effect of each compound on PGM surface charge. All error values for data are displayed or written as 95% confidence intervals.

Dynamic Light Scattering Particle Sizing. The Nanobrook Omni PALS instrument equipped with Brookhaven Instruments Particle Solutions Software was also used to perform particle sizing via dynamic light scattering (DLS). DLS measurements were collected for the 21 PGM solutions at various concentrations of ChCl, PBA, and TEA. All error values for data are displayed or written as 95% confidence intervals.

3.4. Results and Discussion

The results of the study show that all three compounds have the ability to alter mucin viscoelastic and structural properties, but present conflicting trends when rheological data is compared to zeta potential and particle sizing data. Zeta potential and DLS were coherent in that all three compounds were shown to disrupt mucin aggregation, although potentially through different mechanisms of action. All three can H-bond with mucin domains, but the effects of ChCl and TEA were also influenced by the presence of the Cl^- counterion in ChCl and a large increase in pH at higher concentrations of TEA. These influences may have played a role in the conflicting results seen regarding the viscoelastic behavior of the PGM solutions.

Rheology oscillatory frequency sweeps were used to examine the effects of particle surface chemistry and concentration on the viscoelastic properties of PGM solutions. The addition of choline chloride, with choline being cationic in acidic environments, resulted in a decrease of viscoelastic properties compared to neat PGM solutions (see Ch. 2). This was also connected to a trend of higher values of storage and loss moduli with increasing concentration (Fig. 17). The effect of phenylboronic acid (Fig. 18) is not nearly as clear as the lowest and second highest concentrations tested were shown to cause the greatest increase of the viscoelastic moduli, with concentrations of 2 mM and 0.1 M showing little deviation from values obtained from neat PGM solutions (see Ch. 2). The case for triethanolamine is similar, with the only concentration shown to increase moduli values being 0.01 M (Fig. 19). This increase in viscoelastic properties is not linked with a clear increase or decrease in concentration and is not consistent with pH effects seen in Ch. 2. These would predict a decrease in viscoelastic properties at high enough concentrations of TEA to increase pH above 4. This occurred at concentrations above 2 mM TEA.

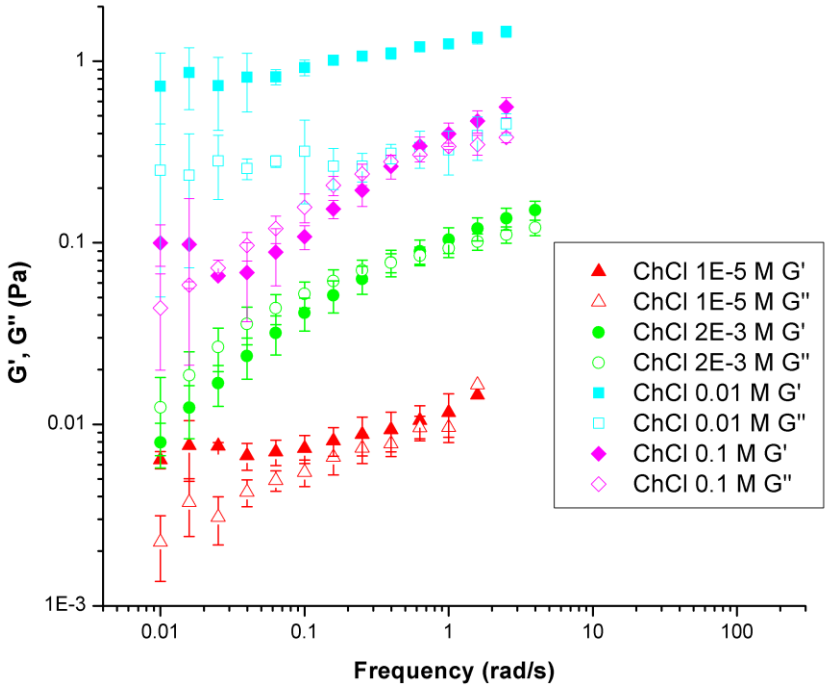

Figure 17. Storage and loss moduli of ChCl-PGM solutions are shown to increase at higher ChCl concentrations.

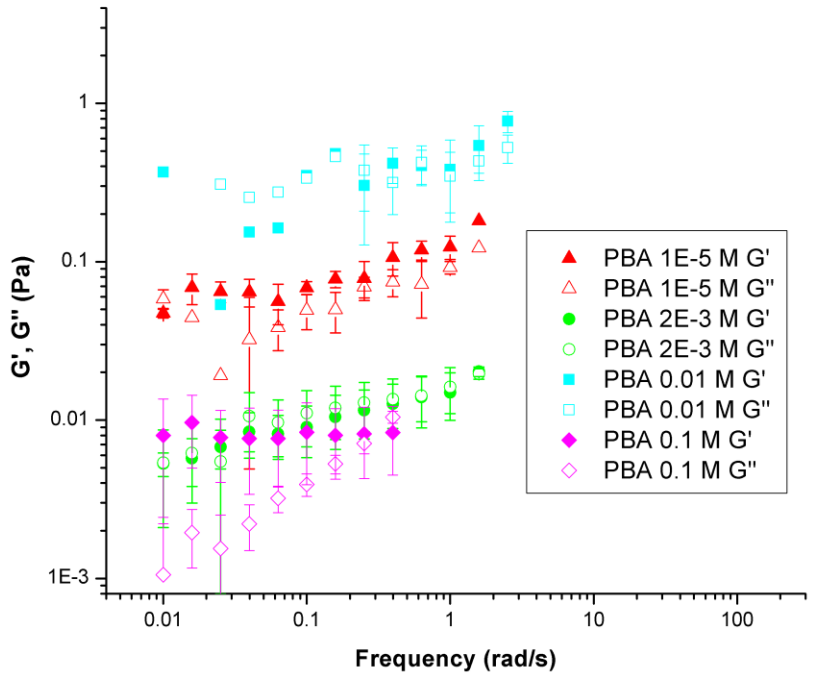

Figure 18. Storage and loss moduli of PBA-PGM solutions are shown to increase at 0.01 mM and 0.01 M PBA.

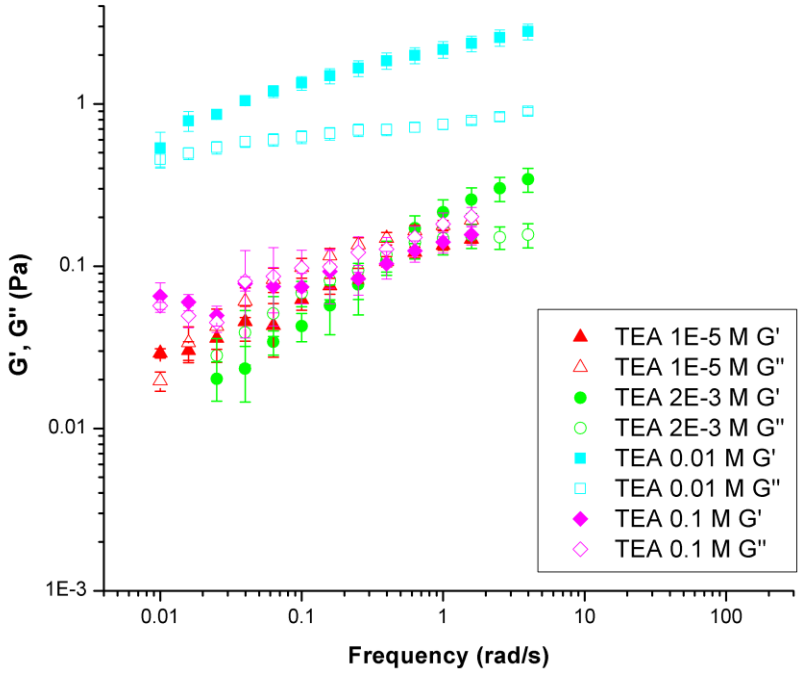

Figure 19. Storage and loss moduli of TEA-PGM solutions are shown to increase at 0.01 M TEA.

Neat PGM solutions have a net surface charge of -6.3 ± 0.30 mV, which can be neutralized at pH values below 4 (see Ch. 2). At concentrations less than 2 mM, which is equivalent to ~0.025 w:w ratio of small molecule:PGM, the addition of ChCl, PBA, and TEA showed no effect on the net surface charge (Fig. 20). Solutions with PBA or TEA > 2 mM showed a significant decrease in the net surface charge to -13.31 ± 0.53 mV with PBA and -27.39 ± 0.95 mV with TEA. This decrease in net surface charge indicates a stronger repulsion between mucin fibers, leading to increased electrostatic dispersion and disruption of the network structure. This finding is supported by other studies which have examined the effect of negatively charge carboxyl- and positively charged amine-functionalized nanoparticles on mucin solutions[14,24]. Amine-functionalized nanoparticles have also been shown to diffuse more slowly through both native and purified mucin solutions than carboxylate-functionalized particles, with Crater and Carrier concluding that transport rates through mucin solutions are inversely related to the surface charge of particles[56]. This suggests that positively charge compounds have mucoadhesive properties, which increases the potential for amine groups to change normal mucin properties, as seen with TEA in this study. This dispersion effect is important for applications where it is necessary to disrupt mucin-mucin interactions to allow a material to diffuse more quickly across a mucus lining (e.g., drug delivery) or lower the viscosity to allow for ciliary clearance (e.g. therapeutics for cystic fibrosis).

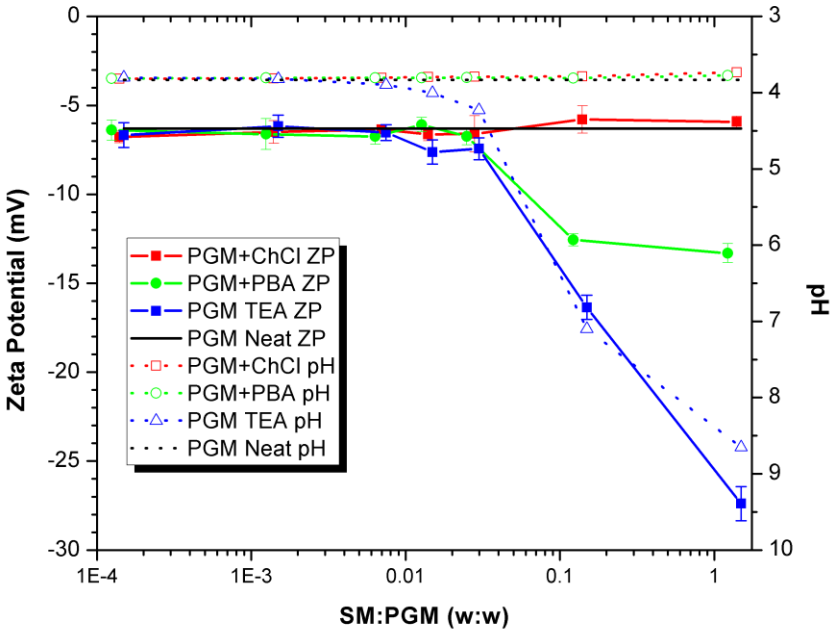

Figure 20. Zeta potential and pH of PGM solutions. PBA and TEA caused large decreases in surface charge at concentrations above 2 mM. Zeta potential changes upon TEA addition correlate to large increases in solution pH.

Examining the zeta potential values more closely, it is clear there is an inverse correlation between the zeta potential of each small molecule dissolved in water and the maximum zeta potential observed in PGM solutions (Table 2). Choline chloride, which is highly electronegative in aqueous solution, had little effect on the surface charge of PGM molecules, even at high concentrations. The choline cation was expected to have mucoadhesive properties with the ability to disrupt mucin structure through electrostatic effects, but this was not observed through zeta potential characterization. The accompanying chloride cation may have played a role in neutralizing any changes in zeta potential related to interactions between choline and PGM molecules. Increased salt concentration is known to induce this neutralizing effect on the zeta potential of biomolecules like PGM[95]. The amphiphilic properties of choline cannot be completely overlooked and is worth further inspection in the future. At high concentrations PBA and TEA were shown to decrease the net surface charge of PGM significantly, with TEA having a much more significant effect. PBA's alcohol groups likely achieved this effect through H-bonding with mucin domains, breaking disulfide bridges and interfering with intramolecular bonding. TEA likely has a similar mechanism, but also benefits from the synergistic effect of increased pH, which decreases mucin aggregation and induces solution-like behavior.

Table 2. Zeta potential of aqueous PGM solutions with addition of each compound. "H_2O only" indicates values taken for the small molecules dissolved in water with no added PGM.

Choline Chloride (ChCl)			Phenylboronic Acid (PBA)			Triethanolamine (TEA)		
Sample	Zeta Potential (mV)	95% CI (mV)	Sample	Zeta Potential (mV)	95% CI (mV)	Sample	Zeta Potential (mV)	95% CI (mV)
C1	-6.78	0.33	P1	-6.39	0.57	T1	-6.67	0.70
C2	-6.50	0.64	P2	-6.62	0.87	T2	-6.17	0.63
C3	-6.35	0.26	P3	-6.75	0.43	T3	-6.53	0.45
C4	-6.63	0.35	P4	-6.09	0.40	T4	-7.62	0.68
C5	-6.60	1.02	P5	-6.75	0.46	T5	-7.44	0.62
C6	-5.79	0.76	P6	-12.56	0.34	T6	-16.36	0.68
C7	-5.93	0.31	P7	-13.31	0.53	T7	-27.39	0.95
H_2O only	-37.08	0.74	H_2O only	-24.03	3.92	H_2O only	-7.06	1.81

To further understand the effect of these compounds on mucin properties, dynamic light scattering (DLS) was used to determine the particle size at various compound concentrations. Measurements illustrated significant heterogeneity for lower concentration samples (Fig. 21) and provided useful information regarding PGM aggregation. Mucin particle size was shown to be reduced significantly from ca. 1 μm to less than 300 nm for all three compounds at high concentrations (>10 mM). ChCl, PBA, and TEA have respective pKa values of 12.5 (predicted using ChemDraw™) , 8.9[87], and 7.76[88] meaning that all should exist in cationic form in aqueous solutions. TEA is a strong base, increasing the pH of solutions at 2 mM to 4 and greater, a regime where PGM is known to have solution-like behavior and have decreased particle aggregation. Also, interaction with bound sialic acids in PGM may allow these molecules to behave as anionic particles in local mucin domains, inducing a reduction in mucin aggregation due to its general electronegativity. It is also possible these compounds are interacting with and occupying terminal cysteine groups on mucin molecules and preventing intermolecular disulfide bonding in PGM.

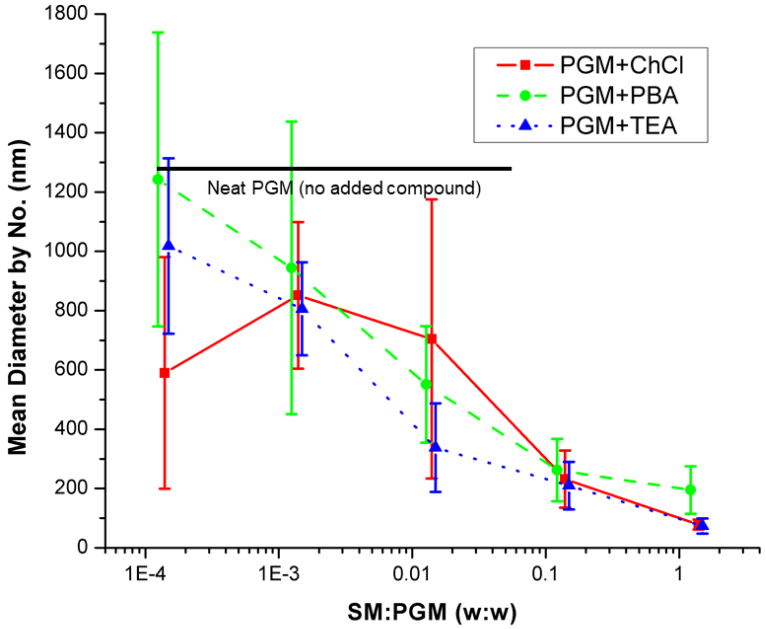

Figure 21. Mean PGM hydrodynamic diameter decreased with the addition of all three compounds. At 10 mM, D_H had been reduced by ca. 70%.

Particle diameter data (Fig. 21) show that at concentrations greater than 0.1 mM for all three probe molecules the mucin average hydrodynamic diameters decreased. This indicates more condensed conformations were induced by the addition of the probe molecules and so mucin-mucin interactions (and resulting network structures) were diminished. The small probe molecules may have served to disrupt electrostatic and hydrophobic interactions between mucin chains, decrease their surface charges and promoting dispersion. It is also possible that the added compounds affect disulfide bonding between mucin monomers, which would cause a decrease in particle size as well.

A previous study by Saitoh et al. on the binding of tertiary and quaternary ammonium compounds to gastric mucin concluded that tertiary amines like TEA had strong binding to mucin, while quaternary ammonium compounds like ChCl did not[96]. Their finding regarding binding affinity may be correct, but ChCl caused a clear decrease in average particle size across all concentrations, which points to some significant interaction, although this could be a result of the chloride content, which is known to cause swelling and increase dispersion of mucin[32]. Excepting the PGM-TEA solutions at concentrations at 0.01 M and above (last two data points in Fig. 20), the pH values for the solutions with ChCl, PBA, and TEA are nearly identical to the value of ca. 4 for a neat PGM solution at 10 mg/mL. Based on comparison to the neat PGM control sample, the change in particle diameter in these solutions is concluded to be a result of the addition of the small molecule compounds and not due to changes in pH. The TEA solutions, as mentioned, did have increased pH at higher concentrations, but the particle diameter was shown to decrease even

at lower concentrations before the increase in pH, implying that the electrostatic effects of TEA played a significant role in hindering mucin aggregation.

3.5. Conclusions

Mucin behavior is incredibly complex, involving electrostatic and hydrophobic interactions between mucin protein domains via intra- and intermolecular bonding. The surface chemistry of compounds applied to PGM solutions is very important in determining the effect on mucin properties, but the effects of ion content and pH can also be significant. Choline chloride, a monovalent ammonium salt, was shown to increase mucin viscoelastic property values at concentrations above 10 mM and zeta potential data support the potential for higher levels of mucin aggregation. These results were conflicted by particle sizing measurements, which showed a clear decrease in particle size at higher concentrations of ChCl. Clearly, the effect of the chloride counterion needs to be further investigated in addition to the amphiphilic nature of the choline ion. PBA and TEA also produced interesting results. PBA, with two alcohol functional groups was shown to decrease viscoelastic properties at 2 and 10 mM, but values were increased at 100 mM. This result conflicts with the clear correlation between decreasing zeta potential and particle size with the addition of higher concentrations of PBA. TEA was shown to increase viscoelastic properties at just one concentration (10 mM), but also drastically increased solution pH to 7 and above at concentrations of 10 and 100 mM. The increase in viscoelastic properties at 10 mM TEA seems anomalous as this increase in pH, coupled with decreasing zeta potential and particle size should correlate to decreased viscoelastic property values.

From this study, all three compounds are recommended for further investigation and future is in the functionalization of nanoparticles for mucus-related applications. The rheological data should be re-examined and an attempt should be made to decouple the effects of counterions and pH in ChCl and TEA.

Chapter 4. Physicochemical Characterization of Mucin Interaction with Silica Nanoparticles

4.1. Abstract

The Stöber process, developed in 1968, is one of the most widely used techniques to synthesize uniform silica nanoparticles (SiNPs) and control their properties. This work describes the method used to produce SiNPs with particle diameters of 74.79 ± 21.80 nm. These particles were then incorporated into aqueous solutions of porcine gastric mucin (PGM), whose physicochemical properties were interrogated using rheology, zeta potential, dynamic light scattering. SiNPs were shown to induce a significant decrease in storage and loss moduli of neat PGM solutions, which point to a decrease in mucin aggregation. Addition of SiNPs also decreased PGM surface charge from -6.30 ± 0.30 mV to -12.90 ± 0.34 mV, indicating dispersion which was confirmed by a decrease in PGM particle size of ca. 70%.

4.2. Introduction

Mucus is an important complex fluid found in the epithelia, digestive, respiratory, and genital tracts of vertebrate animals. It is also present in invertebrates, serving a number of purposes like navigation, defense, hydration, structural support, food, and movement. In humans, it plays a critical role in protecting the body from particulate matter, bacteria, viruses, and harmful chemicals. Mucin, the main functional molecule in mucus, is a biopolymer responsible mucus structure, aggregation, and transport properties.[9] The type of mucin and location within the body influences the microstructural, mechanical, and transport properties of mucus, making the study of mucin vital to the advancement of many fields, including drug delivery, mucus-related disease treatment, and treatments of certain forms of cancer.[21,24,79]

Prior studies have examined the development of polymer and nanoparticle chemistries for use in various biological applications related to mucus.[15,23,42,52,75,80,97–99] Specific areas of focus include mucoadhesion, swelling, and dispersion of mucus and mucin solutions in response to applied polymeric or nanoparticle chemistries or changes in the chemical environment through pH or ion concentration.[5,15,24,31,38,99–102] Many of the studies in this field use gold or silica nanoparticles as a substrate for chemical functionalization, which makes it necessary to evaluate the individual contribution of the nanoparticle itself when assessing the results of interactions within mucus and mucin solutions. In this study, the Stöber process used to synthesize silica nanoparticles (SiNPs) will be described and these SiNPs will be incorporated into mucin solutions in order to assess their contribution—as solid nanoparticle inclusions and sources of SiOx (e.g., SiOH, SiO_2) groups—in changing the physicochemical properties of mucin aqueous solutions.

4.3. Materials and Methods

Silica Nanoparticle Synthesis, Characterization, and Preparation. Silica nanoparticles were synthesized using a modified Stöber process[103,104] (Fig. 22) using 100 mL of ethanol (EtOH,

anhydrous, ≥99.5%, Sigma Aldrich), 6 mL of ammonium hydroxide (NH_4OH, ACS reagent, 28-30%, VWR), and 8 mL of tetraorthosilicate (TEOS, $Si(OC_2H_5)_4$, 98%, Sigma Aldrich). Reactants were combined and stirred over a 24-hour period to produce uniform, monodisperse SiNPs, as shown in Fig. 23.

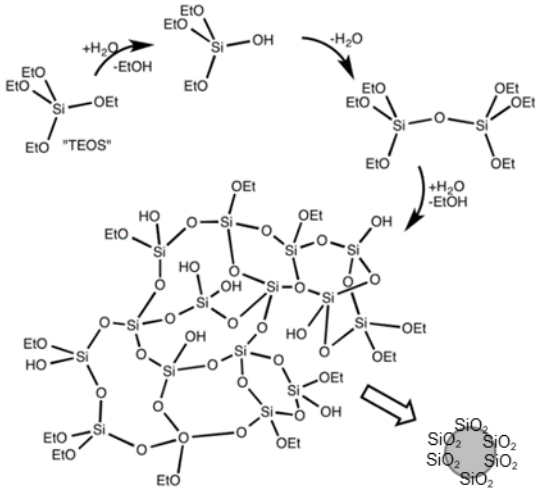

Figure 22. Simplified schematic of the Stöber process reaction schematic showing hydrolysis and condensation of TEOS. Adapted from Wikimedia Commons[105].

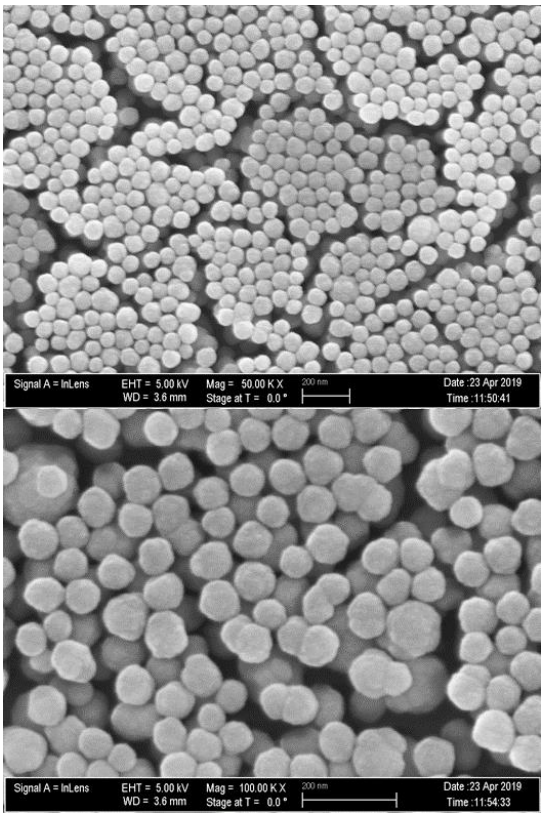

Figure 23. SEM micrographs of SiNPs produced using Stöber process show a fairly uniform particle size of 77.3 ± 5.7 nm.

The reaction mixture was stirred for 24 hours, after which it was dried using rotary evaporation. The SiNPs were suspended in 20 mL of Nanopure™ water and sonicated for 30 minutes and unreacted TEOS was removed using Spectrum™ Spectra/Por™ 1 RC dialysis membrane tubing (6000-8000 Dalton MWCO). The suspended SiNP solution was loaded into the dialysis tubing, which was then placed in Nanopure water at a 1:100 v/v ratio of SiNP solution:water. The water was heated to 40°C with continuous stirring, and the water replaced at 1, 3, 6, and 20 hours. After dialysis, the SiNP solution was dried in an oven at 70 °C, weighed, resuspended in water at 10 mg/mL, and then sonicated for 30 minutes.

Dilute SiNP solutions at approximately 0.05 mg/mL in water were prepared for baseline characterization using DLS and zeta potential. 0.05 mg/mL solutions were also prepared in isopropanol to be used in FTIR characterization.

Silica nanoparticles produced from this process had an average particle diameter of 77.3 ± 5.7 nm as shown by SEM imaging (Fig. 23) and measured using open source ImageJ software. DLS measurements showed good agreement with the SEM data, with an average hydrodynamic

diameter of 74.79 ± 21.80 nm. The net surface charge was measured using zeta potential to be -26.79 ± 3.34 mV, which agrees fairly well with the literature value for SiO_2 powder[106] of approximately -30 mV. Although it should be noted that Klapiszewski et al. have measured values ranging around -15 mV for SiNPs synthesized with the Stöber process at the same pH value (5.4) with average particle diameters between 290 and 295 nm[104,107,108]. Sun et al. have produced SiNPs also using the Stöber process with average diameters between 243 and 823 with zeta potential values from -39.1 to -31.0 mV at pH 7.4[108]. Zeta potential of SiNPs is known to decrease at higher pH values, and it is clear from the work of Sun et al. that smaller particles have lower zeta potential values. Taking into account these effects of pH and particle size as well as the good agreement between the literature value for zeta potential of silica powder, the synthesis process described was determined to be successful. The zeta potential value measured for our synthesized SiNPs is also in good agreement with the zeta potential of phenylboronic acid (see Ch. 3), a compound whose chemical structure is dominated by two -OH groups, which is very similar to silica.

FTIR spectroscopy (Fig. 24) was used to confirm the chemical structure of the synthesized silica nanoparticles (SiNPs). The strongest peaks were assigned as Si-O asymmetric stretching (1250-1000 cm^{-1}) and Si-O-Si bending at 467 cm^{-1}. Si-OH asymmetric and Si-O symmetric stretching are seen at 950 and 795 cm^{-1}. More subtle O-H stretch peaks are observed at higher wavenumbers for mutually hydrogen-bonded SiNPs at ~3660 cm^{-1} and Si-OH hydrogen-bonded with water at 3550-3300 cm^{-1}. This slight water absorption (likely from adsorbed water) is confirmed by the short OH bending peak at 1635 cm^{-1}. There is also asymmetric and symmetric stretching for CH_3 at 2956 (as) and 2867 (s) cm^{-1} and CH_2 at 2920 (as) and 2855 (s) cm^{-1}, which is evidence of remaining ethoxy groups on TEOS molecules that were not fully reacted.

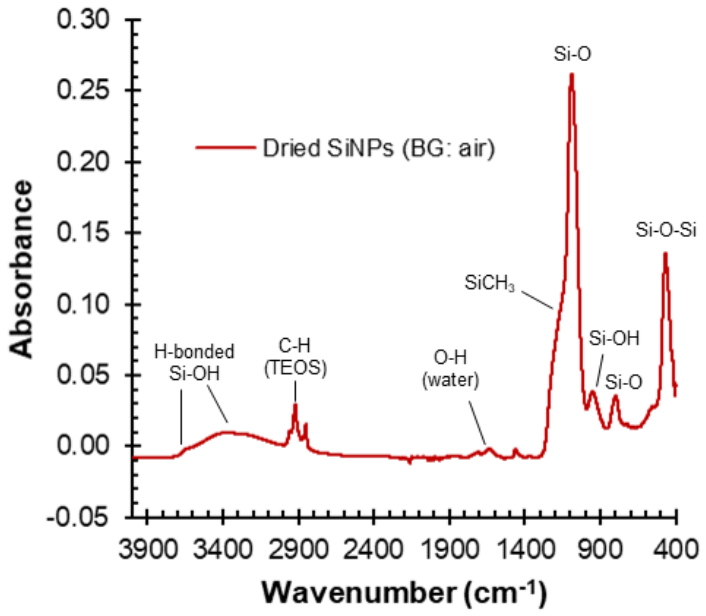

Figure 24. FTIR spectra for Stöber-synthesized SiNPs confirms the particle structure, with only a small amount of unreacted TEOS.

Table 3. IR wavenumber assignment for functional groups present in the Stöber-synthesized SiNPs.

Wavenumber (cm^{-1})	Bond Assignment
3660	H-bonded Si-OH (mutual) and Si-OH stretching
3550-3300	Si-OH stretching, H-bonded to water
2956-2855	C-H stretching of unreacted TEOS
1635	O-H bending of water
1250-1000	Si-O asymmetric stretching
950	Si-OH asymmetric stretching
795	Si-O symmetric stretching
467	Si-O-Si bending

SiNP-Mucin Solution Preparation. Porcine gastric mucin (PGM, Type II, Sigma Aldrich) was used to create solutions at 10 mg/mL, to which various amounts of SiNPs were added to study the effect of concentration on mucin properties. Six samples were prepared at the concentrations listed below (Table 1) and sonicated for 30 minutes. The neat PGM solution (B) had a pH value of 4.1.

Table 4. Summary of PGM solutions with various amounts of added SiNPs.

Sample	PGM Conc. mg/mL	SiNP Conc. mg/mL	SiNP:PGM w:w
B	10	0	0
2	10	2	0.2
1	10	1	0.1
0.5	10	0.5	0.05
0.3	10	0.3	0.03
0.1	10	0.1	0.01

Rheology. Rheological data was collected using a Discovery Hybrid Rheometer II (DHR-2, TA Instruments) equipped with a 40 mm cone and plate geometry (2.013° angle and 53 μm gap) and temperature-controlled Peltier plate. All runs were completed at 25 °C.

Oscillatory amplitude sweeps were run to find the viscoelastic region of each ample, which is required before running a frequency sweep. Each sample was then characterized using frequency sweeps over a range of 0.1-100 rad/s.

Dynamic Light Scattering. DLS particle sizing results were obtained with a Nanobrook 90Plus (Brookhaven Instruments) using polystyrene sample cuvettes. Samples were sonicated for 30 minutes plus an additional 2 minutes immediately prior to data collection. Solutions were diluted approximately 200x and run at 25 °C.

Zeta Potential. Zeta potential results were obtained with the same Nanobrook 90Plus using Phase Analysis Light Scattering (PALS) functionality. Data were collected using 30-cycle measurements at 25 °C.

FTIR. FTIR spectra were obtained using a Thermo Fisher Nicolet iS50 instrument with a deuterated triglycine sulfate (DTGS) detector, attenuated total reflectance (ATR) accessory with diamond-ZnSe crystal and a XT-KBr beamsplitter. SiNPs in isopropyl alcohol and SiNP:PGM solutions were drop-cast onto the ATR crystal for measurements at ambient temperature (approximately 23 °C).

4.4. Results and Discussion

The rheology frequency sweep data (Fig. 25) for all samples except the neat PGM solution is only shown for frequencies less than 1 rad/s. The data sets were developed from three frequency sweeps and each had issues with inertia correction at frequencies greater than 1 rad/s for solutions when SiNPs were added. (Note that inertia correction issues occurred at frequencies greater than 10 rad/s for the neat PGM solutions.) Above each of these inertia correction cut-off frequencies, the raw phase angle (measured by the rheometer) was 175° or greater. For the DHR-2 rheometer, this is the upper limit for inertia correction. Since data collected above this upper limit is not reliable, it was omitted in Fig. 25. Inertia correction must be examined with all rheology measurements at high frequency, especially in lower viscosity samples. At high frequencies, if the raw phase angle (measure and reported by the TA Instruments DHR-2) is greater than 175°, then that data point should be truncated. The neat PGM sample required truncation above 10 rad/s, whereas the SiNP-doped solution data had to be truncated at 1 rad/s. This suggest that the viscosity of the solutions with SiNPs are lower than the neat PGM solution, which is also confirmed by the decreased storage and loss moduli in these samples.

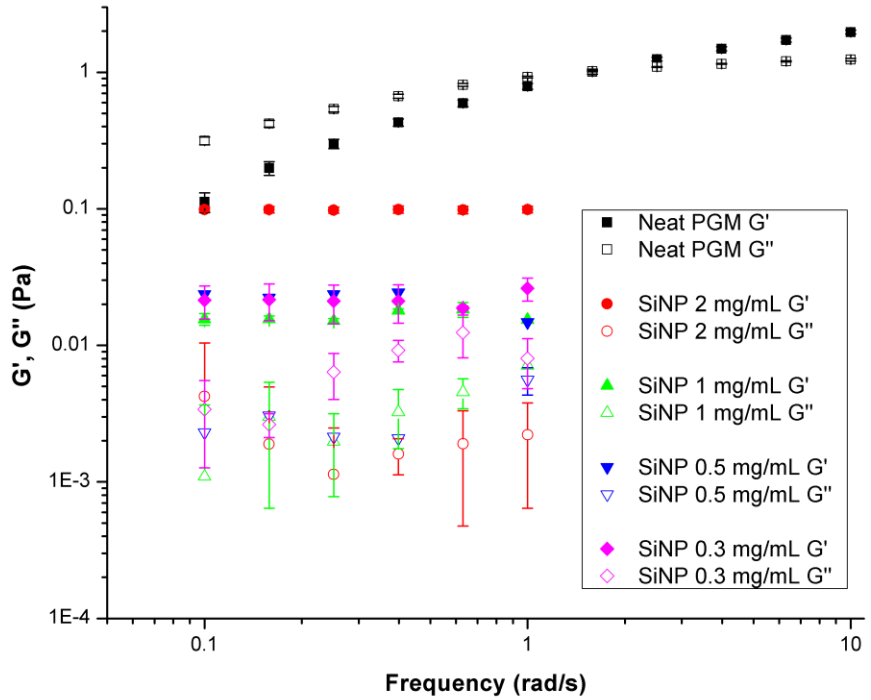

Figure 25. Frequency sweeps indicate a decrease in viscoelastic properties for all PGM samples doped with SiNP at 10 mg/mL.

The frequency sweep data sets in Fig. 25 show the viscoelastic behavior of the neat PGM solution (pH 4.1) at low frequencies is dominated by the loss modulus (G'’). This liquid-like behavior at low frequency values suggests that the sample is in the solution regime, only displaying gel-like behavior above 1 rad/s, where the storage modulus (G’) dominates. This behavior is in direct contrast to the PGM solutions doped with SiNPs, which all display gel-like behavior over the same frequency range. In addition, it is seen that the viscoelastic moduli do not change significantly for samples with SiNP concentrations between 0.3 and 1 mg/mL. At 2 mg/mL, the storage modulus increased to a value approximately five times that of the other samples. The notable decrease in the loss modulus of mucin solution may be a result of mucin aggregation around SiNPs, which could account for the frequency-independent solid-like behavior displayed at all concentrations. The overall rheological behavior may also indicate that there is bonding taking place between Si-OH groups and mucin domains to promote mucin transition to the gel regime, in which mucin fibers are seen to aggregate into small clusters[37]. This stabilization through weak H-bonding, however, would also be accompanied by electrostatic repulsion which serves to reduce the viscoelastic behavior of PGM solutions overall. This likely takes place through repulsive effects in which mucin aggregates are pushed away from one another and intramolecular bonding is reduced.

The dispersion of mucin particles is supported by particle sizing measurements (Fig. 26), which illustrate a strong connection between the presence of SiNPs and a decrease in mucin size. All solutions were polydisperse, so average hydrodynamic diameters are reported with relatively

large 95% confidence intervals. There is a strong correlation between SiNP concentration and a decrease in particle size. This supports the hypothesis that SiNPs have a disrupting effect on mucin domains and that the frequency-independent and dominant storage moduli seen in rheology (Fig. 25) are a result of a nanoparticle-dominated viscoelastic character in the solutions.

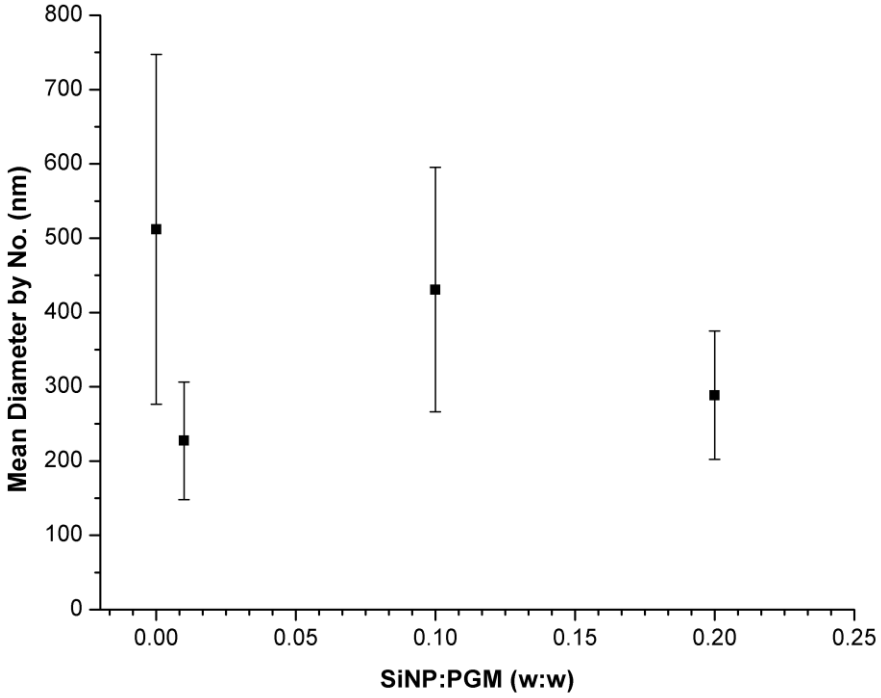

Figure 26. Dynamic light scattering measurements show decreased mucin size with increased SiNP loading.

Zeta potential measurements further support the idea that the addition of SiNPs promotes dispersion of mucin particles. PGM has a negative surface charge and the zeta potential of PGM solutions is -6.30 ± 0.30 mV. With the addition of SiNPs, the surface charge decreased to a minimum of approximately -12.90 ± 0.34 mV at SiNP:PGM ratios of 0.1 (w:w) and higher, shown in Fig. 27. Other researchers have shown that positively charged particles are generally mucoadhesive, decreasing swelling and dispersion and the opposite effect is observed for negatively charged particles, which excel more strongly in terms of mucopenetration[14,23,24,109]. The trend towards a more electronegative surface charge in this study supports the claim that negatively-charged SiNPs discourage aggregation of PGM particles and likely have better mucopenetrating ability than positively-charged particles. This is also supported by large decreases in zeta potential with the addition of phenylboronic acid and triethanolamine, which both contain -OH functional groups (see Ch. 3).

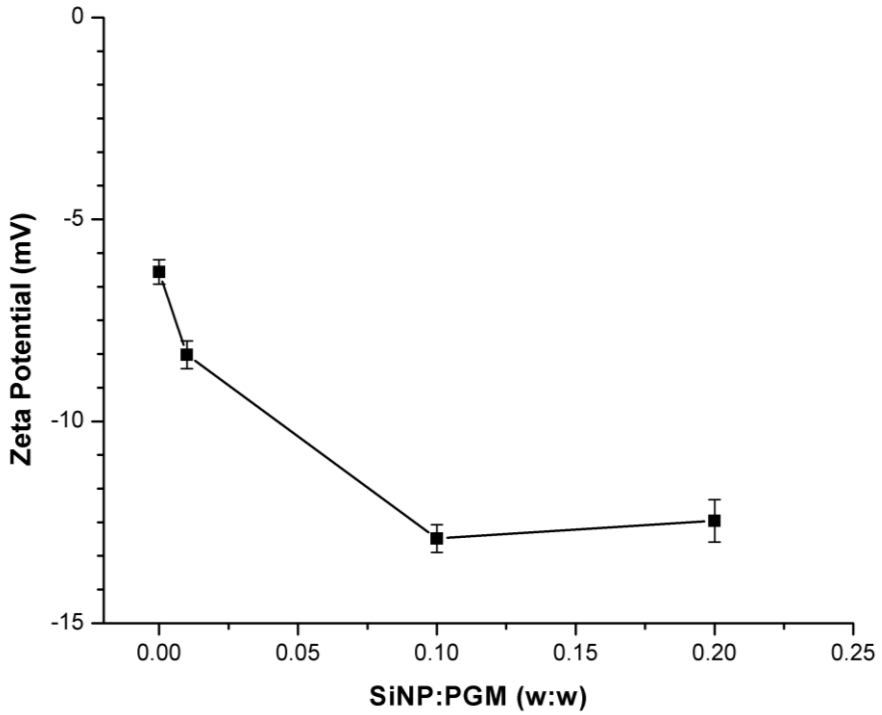

Figure 27. Zeta potential measurements of PGM-SiNP solutions decrease surface charge as a function of SiNP loading.

The changes seen in rheology, DLS, and ZP measurements were expected due to the electronegativity of silica nanoparticles, which predicts repulsion from the large negatively charged domains in PGM. From these data, it is suggested that the effects of SiNPs on PGM solutions seen through these techniques are due to electrostatic effects, where the presence of SiNPs increases repulsion and limits self-interaction between PGM domains. These effects match generally with the results found in the examination of small molecule compounds (see Ch. 3), specifically, the decrease in particle size and zeta potential with increasing concentrations of added molecules. The results provide further evidence supporting the idea that electrostatic forces are a driver of mucin aggregation and structural properties[9,42,97,110,111].

4.5. Conclusions

This study served multiple purposes, the first of which was a demonstration of a successful method to easily synthesize small (~75 nm) silica nanoparticles with good uniformity. Silica nanoparticles provide a perfect substrate for chemical modification in the form of surface functionalization or functionalized polymer growth. However, it is first necessary to understand the effect of adding another phase, solid nanoparticles, on the viscoelastic and physicochemical properties of mucin solutions. This was demonstrated through the addition of SiNPs to PGM solutions at various concentrations. At all concentrations, viscoelastic properties, particle size, and zeta potential decreases (away from neutral), point towards SiNP addition promoting dispersion

of mucin particles and decreasing intramolecular bonding. This dispersion and decrease in particle aggregation match the findings from Ch. 3 regarding -OH functionalized compounds and previous research focusing on the effects of negatively and positively charged particles. Future work should be aimed toward functionalization of SiNPs via silane self-assembled monolayers and/or grafted polymer brushes in order to add specific functional groups and functional group densities on the NP surface in order to further assess the ability of functionalized NPs to significantly alter the mucin structure.

Chapter 5. Conclusions and Future Work

5.1. Study Conclusions

The findings from the work described here contribute positively to the understanding of mucin and mucin-related systems, especially with regards to the effect of pH, divalent ions, charge molecular compounds, and unfunctionalized silica nanoparticles.

The effects of pH and $CaCl_2$ on PGM solutions were clearly demonstrated and confirmed prior findings by other research groups. The addition of 10 mM $CaCl_2$ induced a clear increase in viscosity for solutions at pH 4.0 and 5.8, indicating that Ca^{2+} has the ability to collapse a mucin network and induce gelling behavior. The sol-gel transition was seen to take place at a pH of 4, at and below which PGM solutions displayed gel-like behavior. With the addition of $CaCl_2$, the sol-gel transition was seen to increase significantly, with gel-like behavior taking place at a pH of 5.8. DLS measurements did not show effects related to the presence of $CaCl_2$, but showed an approximate 5-fold decrease in mucin particle diameter at pH values above 4.0. The gelling behavior of PGM at pH values <4 were also confirmed with zeta potential measurements, which indicate the isoelectric point of mucin is approximately pH 2.75. This value was increased to pH 3.1 with the addition of $CaCl_2$, which supports the changes that took place with regards to viscoelastic behavior. $CaCl_2$ induces mucin aggregation through promoting bonding between PGM carbohydrate side chains, a process known as glycosylation.

To inform future work with functionalized particles, the effects of various functional compounds and silica nanoparticles on mucin properties were characterized. The surface chemistry of molecules applied to mucin plays a large role in controlling mucin properties and must be considered in addition to the effects of pH and ion content. Quaternary ammonium compounds like choline chloride have been demonstrated in the past to have lower mucoadhesion than other compounds, but this study showed that may not always be the case. ChCl seemed to have conflicting effects on mucin solutions, increasing viscoelastic properties and decreasing particle size at higher concentrations all while maintaining a surface charge close to that of un-modified PGM solutions. Triethanolamine, a tertiary amine, known for mucoadhesive properties, caused an increase in PGM viscoelastic moduli at 10 mM, which conflicted with a strong decrease in surface charge and particle size which correlated clearly with increasing concentrations. TEA is a strong base which increased solution pH above 4 at concentrations higher than 2 mM. The effect of the pH change on PGM aggregation cannot be ignored, but the changes in zeta potential and particle size were also demonstrated at pH values closer to that of neat PGM solutions. Phenylboronic acid has two -OH groups and induced a general decrease in PGM viscoelastic behavior, which was accompanied by a strong correlation between concentration and decreased zeta potential as well as particle size.

Silica nanoparticles with a particle size of 74.79 ± 21.80 nm were synthesized via the Stöber method and their effects on PGM solutions were examined. SiNPs have -OH functionalization across their surface with a similar surface charge and functional role as PBA. Their effect on the viscoelastic behavior, surface charge, and particle size of PGM was similar as

well. Viscoelastic moduli were reduced across all frequency values measured and the viscosity of PGM solutions was lowered, a conclusion reached by comparing the data truncation required by instrument correction between neat PGM and PGM solutions with applied SiNPs. The decrease in viscoelastic properties was supported by a decrease in PGM surface charge from -6.30 ± 0.30 mV to -12.90 ± 0.34 mV, indicating decreased aggregation of particles. This dispersion of PGM particles was also confirmed through DLS measurements which illustrated an approximately 70% decrease in particle size with the addition of SiNPs.

5.2. Future Work and Recommendations

Future work should focus on characterizing the effects of functional compounds on mucin solutions, potentially expanding to other mucin types and native mucus samples. FTIR, which was used to demonstrate glycosylation in Ch. 2, has potential to be a good tool for examining changes in chemical bonds in PGM samples. More experimentation with this tool should be done, as strong conclusions regarding the effects of small molecule compounds and nanoparticles were not obtained using the simple method of dropwise collection on the ATR crystal.

In addition to the recommendation in Ch. 3 to re-examine rheological data, it would be helpful to couple macro-scale rheology with micro-rheological techniques as well as diffusion or particle tracking studies. This would help provide connections between observable mechanical properties with micro-scale particle interactions. Future studies should also aim to better control ion content and pH when studying the effects of an individual compound, as this was not done effectively in the case of ChCl and TEA, leading to results that were very likely influenced by anion content and changes in pH.

To expand this research more firmly into the fields of drug delivery and therapeutics, work should be aimed at functionalization of silica and gold nanoparticles through changes in surface chemistry and polymeric growth from these substrates. Positive functionalization should be examined as it relates to mucoadhesion alongside negatively-functionalized particles, which have greater mucopenetrative abilities. Combining these through examination of amphiphilic particles also shows promise and could be used to modulate transport through mucosal layers in the body and subsequent release of a therapeutic.

Appendices

Appendix A: Sample Preparation

Mucin solutions were prepared using porcine gastric mucin (PGM) Type II in powdered form, obtained from Sigma Aldrich (CAS 84082-64-4) and refrigerated continuously between sample preparation times. Nanopure^{TM} water, obtained using a Millipore Synergy® Water Purification System with Biopak® polisher, was used in the preparation of all samples described. The majority of samples were prepared at 10 mg/mL as well as other samples at higher concentrations (15-60 mg/mL), which were used to test the effect of concentration on rheological properties. All solutions were stirred over a period of 4-8 hours, refrigerated overnight, and stirred again to ensure dissolution of PGM in the water. For rheology, FTIR, and surface tension measurements, solutions were tested at their prepared concentration. DLS and ZP measurements were made after diluting 100x to 0.1 mg/mL as higher concentrations resulted in adverse scattering effects that made characterization impossible.

A1. pH and Ca^{2+}-Adjusted Samples

At 10 mg/mL, PGM solutions had pH value of ~3.85, which was then adjusted using nitric acid (HNO_3) and potassium hydroxide (KOH). PGM was added to maintain all samples at 10 mg/mL for each pH value studied. Calcium chloride ($CaCl_2$) was added at 0.01 M in the form of calcium chloride dihydrate (≥99%) obtained from VWR International. pH values were tested for all samples before characterization.

A2. Small Molecule-Doped Samples

Choline chloride (ChCl), phenylboronic acid (PBA), and triethanolamine (TEA) were purchased from ThermoFisher Scientific Chemicals (98+%) were used as received to study their effects on PGM. ChCl and PBA were obtained in solid form and were dissolved in water at 7 different concentrations (0.01 mM – 0.1 M) before powder PGM was added at 10 mg/mL. TEA was received in liquid form and was diluted in water at the above concentrations after which PGM was added at the concentration of 10 mg/mL.

A3. Silica Nanoparticle-Doped Samples

Silica nanoparticles (SiNPs) were synthesized using the Stöber method (described Ch. 4), after which they were dried using rotary evaporation, suspended in water, then sonicated for 30 minutes. Unreacted TEOS was removed through dialysis in a stirred bath at 40 °C, with water replaced at 1, 3, 6, and 20 hours. The solution was then dried at 70 °C, after which the solid particles were weighed and resuspended at 10 mg/mL. This solution was used as a stock solution from which 5 PGM solutions were prepared with SiNP concentrations from 0.1 to 2 mg/mL.

Appendix B: Operating Procedures

B1. Rheology

All rheological data were collected using a Discovery Hybrid Rheometer II (DHR-2) and analyzed using TRIOS software (v4.3), both from TA Instruments. A liquid-regulated Peltier plate was used to maintain a constant sample temperature during each analysis period. Two geometries were tested during initial experiments-a 40 mm flat plate and a 40 mm cone-and the cone was chosen due to its ability to maintain a constant shear rate for each data set. The 40 mm cone had a 2.013° angle and a 53 µm gap and a solvent trap was used for each run to discourage water evaporation.

Flow sweeps were performed at 25 °C over a shear rate of 0.001 to 1 s^{-1} with 5 points per decade. TRIOS software was used to implement steady state sensing for the instrument, which is an automated algorithm used to record the steady-state viscosity at each shear rate. Steady state sensing was set with a maximum equilibration time of 45 s, sample period of 30 s, and a 10 % maximum tolerance.

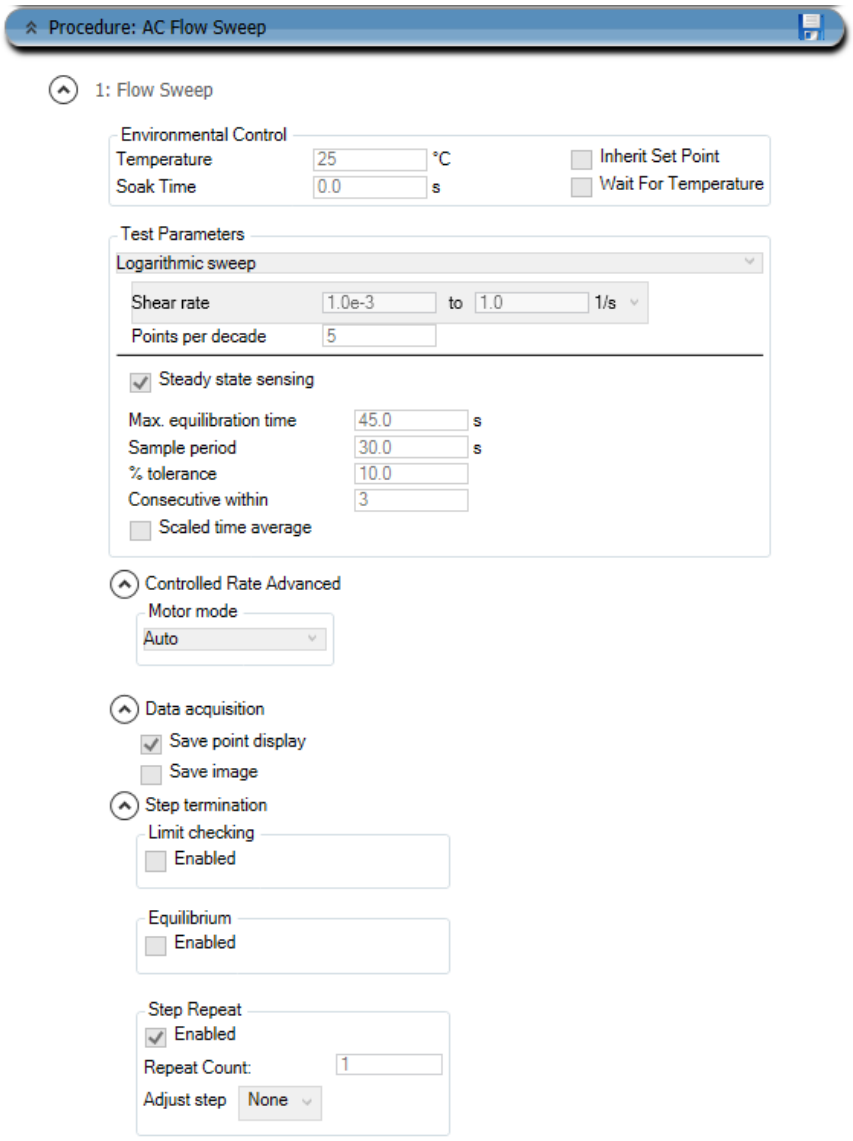

Figure 28. Screenshot from TRIOS procedure panel for flow sweep setup.

Frequency sweeps involved a slightly more difficult process which requires the user to determine the linear viscoelastic regime (LVR) of a sample. This was done to ensure that the measured properties (G' and G'') are independent of the strain induced during the oscillations and also ensure reproducibility and reliability of data. The LVR was determined by performing an oscillating amplitude stress sweep on the sample over a wide stress range (0.001 to 100 Pa). G', G'' and complex viscosity were displayed and examined to find the strain values where their magnitude is constant. From this area, a strain value was chosen and used in the programming of the frequency sweeps. Frequency sweeps were then performed at 25 °C over a range of 0.01 to 100 rad/s.

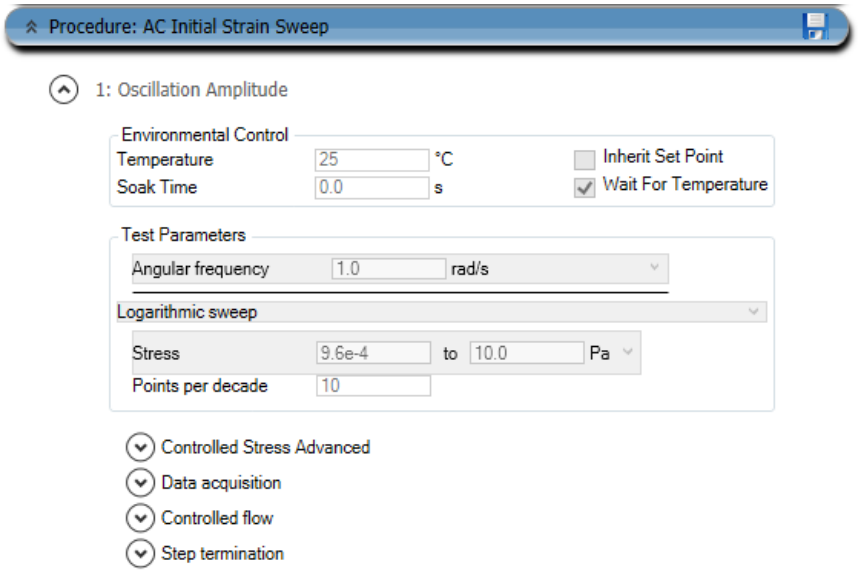

Figure 29. Screenshot of TRIOS procedure pane for stress sweep setup.

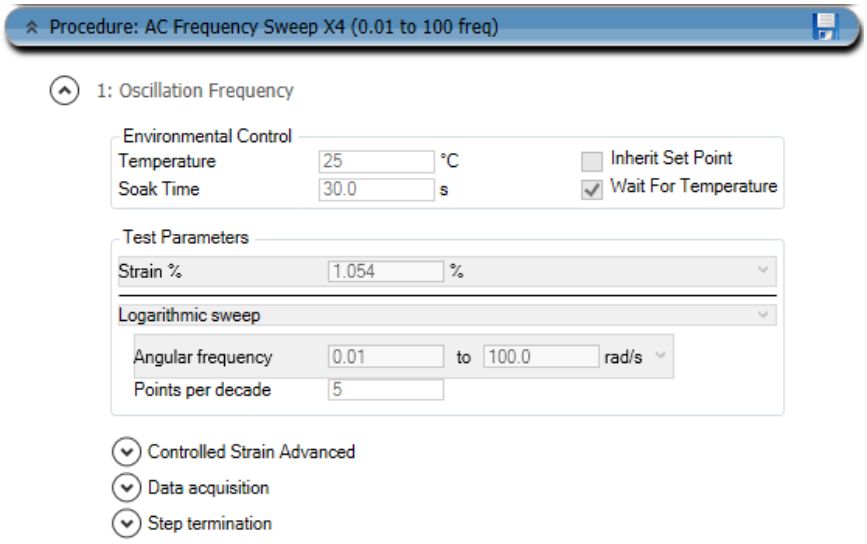

Figure 30. Screenshot of TRIOS procedure pane for frequency sweep setup.

B2. Dynamic Light Scattering (DLS)

DLS data were collected using a Brookhaven Instruments NanoBrook 90Plus PALS (Particle Size & Zeta Potential using Phase Analysis Light Scattering) instrument and analyzed using Brookhaven's Particle Solutions software (v. 3.5). The instrument is equipped at 20 mW 640 nm temperature-controlled red semiconductor laser with an Avalanche photodiode detector. All data were collected using a 90° scattering angle in either disposable, plastic BI-SCP or non-disposable, glass BI-SCGO sample cuvettes. Measurements were performed for each sample over a 90-120 s duration with 10-15 measurements per sample. The refractive index of mucin particles

was set at 1.6116 based on data from Nikonenko et al.[112] Automatic baseline normalization and continuous size distribution were selected and “Globular Proteins” was selected for MW Analysis, although this was not used.

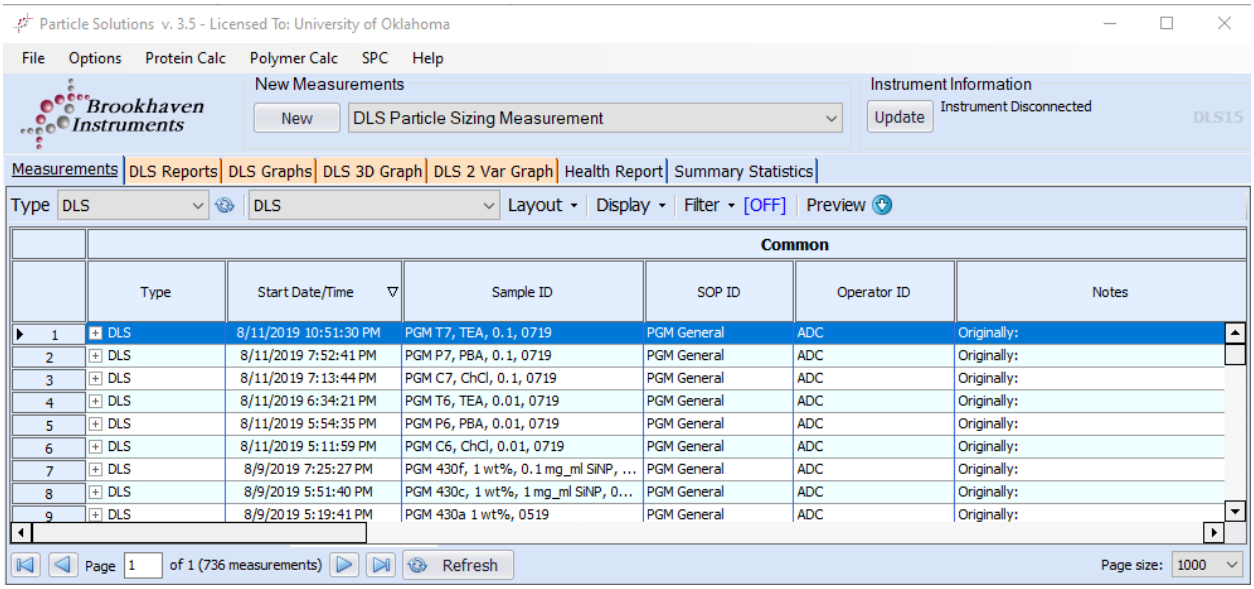

Figure 31. Screenshot of Particle Solutions measurements screen.

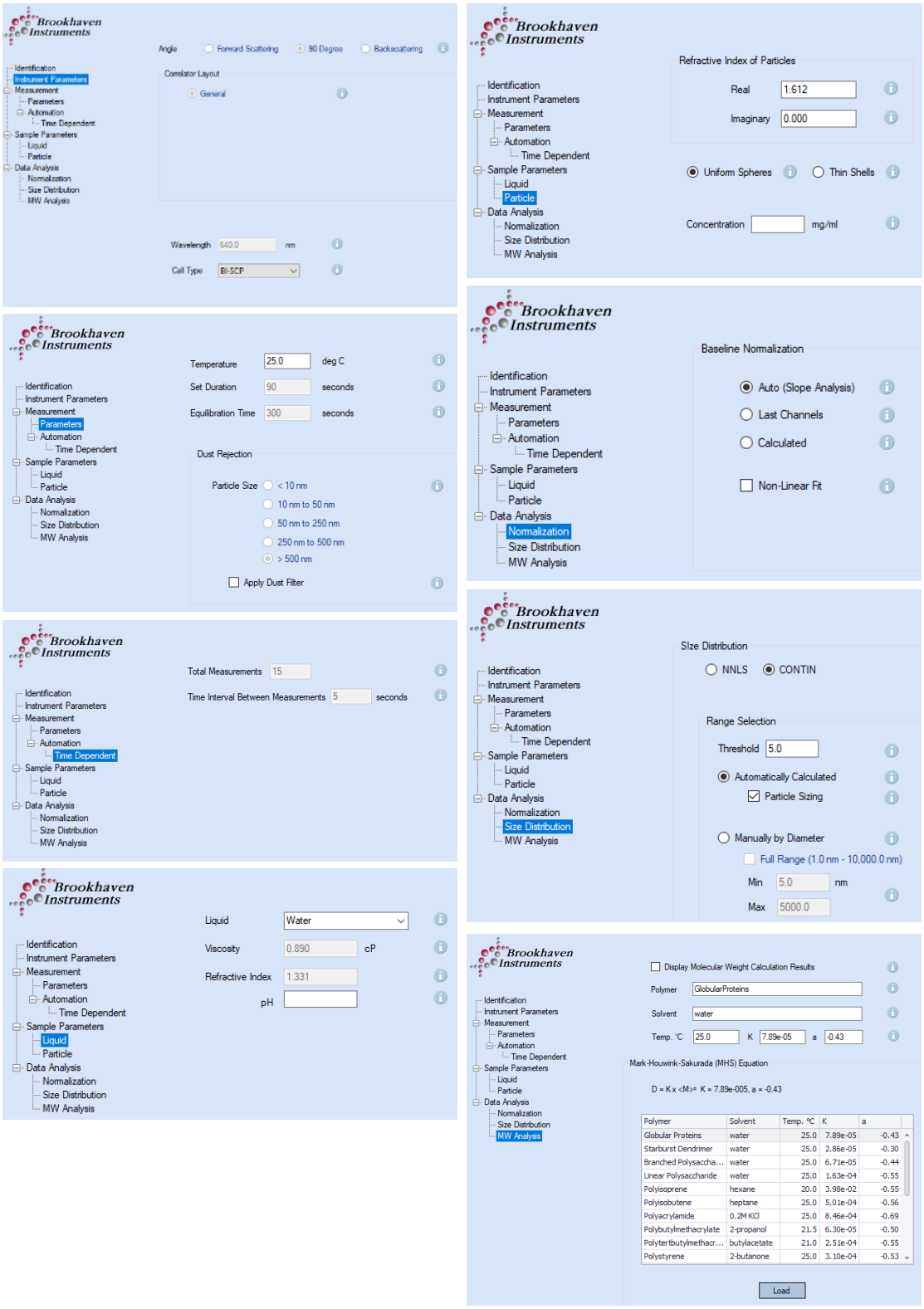

Figure 32. Screenshots from the Particle Solutions SOP Editor for DLS particle sizing measurements.

B3. Zeta Potential (ZP)

ZP data were collected using the same instrument using two different accessories with plastic BI-SCP or non-disposable, glass BI-SCGO sample cuvettes. The BI-ZEL electrode assembly was used to measure the surface charge in individual samples at discrete concentrations and pH values. Measurements were collected at 25 °C using 30 cycles of the electric field and automatic voltage and frequency settings. 5-10 measurements were collected for each sample using the Smoluchowksi ZP model preloaded in the software, which was recommend for large particle sizes (colloids).

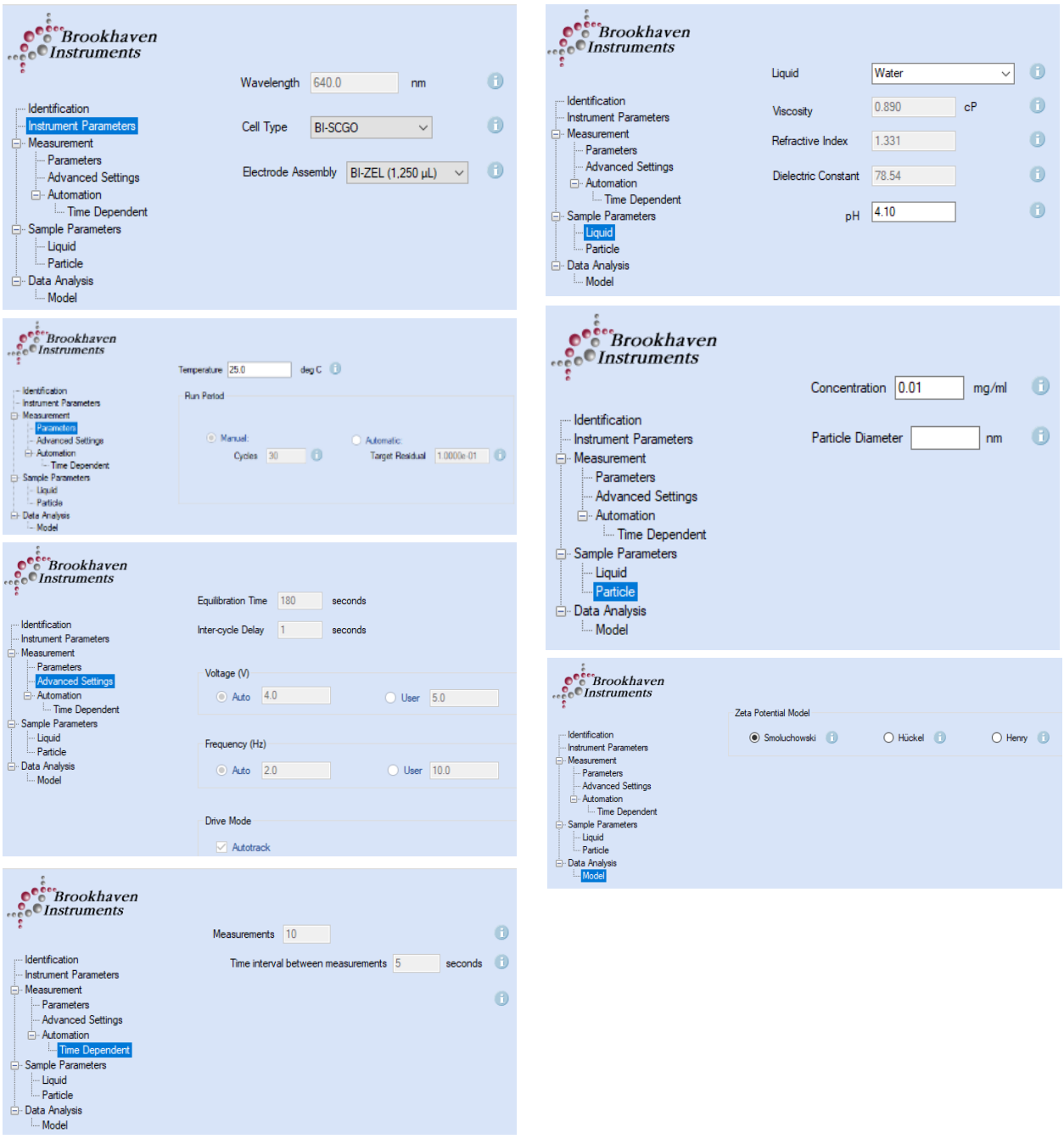

Figure 33. Screenshots from the Particle Solutions SOP Editor for zeta potential measurements.

ZP data were also collected using the BI-ZELF electrode assembly for flow mode, which was connected to the BI-ZTU 4 pump autotitrator with pH probe for regulation. This accessory allowed the collection of ZP data at smaller pH intervals in a manner much more convenient than creating and adjusting individual samples as discrete pH values. The setup for these measurements was very similar; however, only 4 measurements were collected at each pH value, and the "Titration" function was used in the SOP Editor to the desired final pH and number of steps

desired. This required an exact volume of 20 mL to inform the pump controllers, which dispense measured amounts of acid and base (HNO_3 and KOH) to adjust the sample pH.

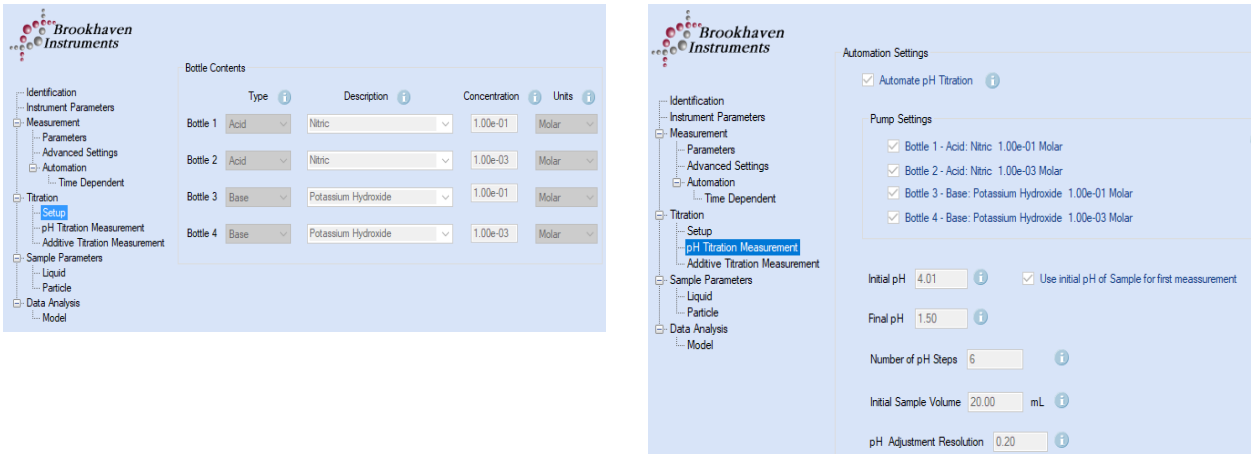

Figure 34. Screenshots from the Particle Solutions SOP Editor for zeta potential titration setup.

B4. Fourier Transform Infrared Spectroscopy (FTIR)

FTIR spectra were collected using a nitrogen-purged Thermo Fisher Nicolet iS50 instrument using a deuterated triglycine sulfate (DTGS) detector, attenuated total reflectance (ATR) accessory with diamond-ZnSe crystal and a XT-KBr beamsplitter. Spectra for samples were collected by dropwise deposition onto the ATR crystal using 256 scans and ambient air as background. The instrument was controlled using Thermo Scientific OMNIC™ software, which was also used to analyze absorbance data. Water was also characterized using an air background and this spectra was subtracted from that of PGM solutions to remove the absorbance bands of water and isolate PGM interactions.

OMNIC was used visualize spectra and identify peak wavenumbers, using the “Find Peaks” feature, shown in Fig. 8.

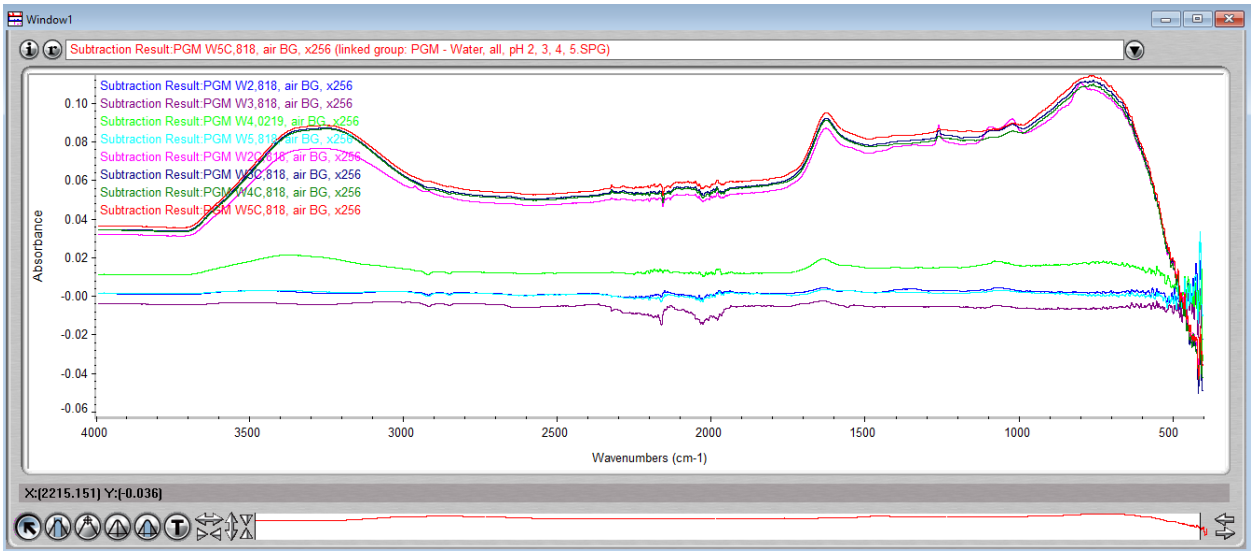

Figure 35. Spectra visualization in OMNIC software.

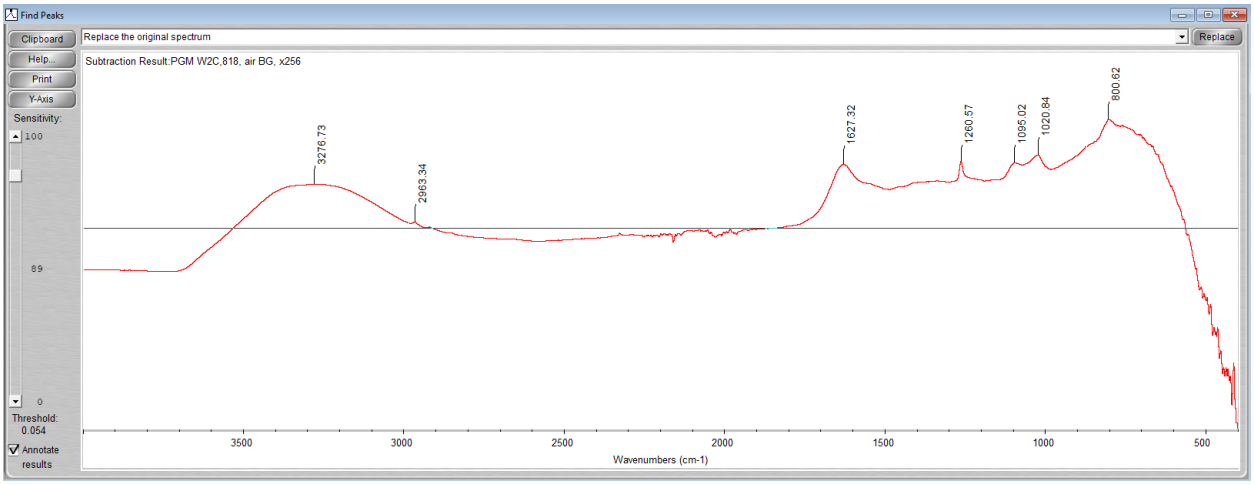

Figure 36. OMNIC software was used to find peak wavenumbers to identify chemical bonds

B5. Surface Tension

Surface tension data was gathered using a Dynamic Contact Angle measuring device and Tensiometer (DCAT) 25 from Dataphysics. All data was measured at 25 °C using an 18.7 mm Du Noüy ring probe made of platinum-iridium. Data was displayed and analyzed using DCATS software and Microsoft Excel. Between each data collection period, the probe heated over a gas-fed flame to decompose and vaporize any sample left from the previous run.

Appendix C: Supplementary Data

C1. Rheology Stress Sweeps

Stress sweeps were not included in the main body of work, as they were not used in a systematic way to study PGM solution properties. They were used primarily to determine the LVR of each solution prior to running frequency sweeps, but also serve to clear demonstrate the shear-thinning behavior of PGM solutions. These data were collected for all samples, but the figures below used as examples are only for the pH and Ca^{2+} samples.

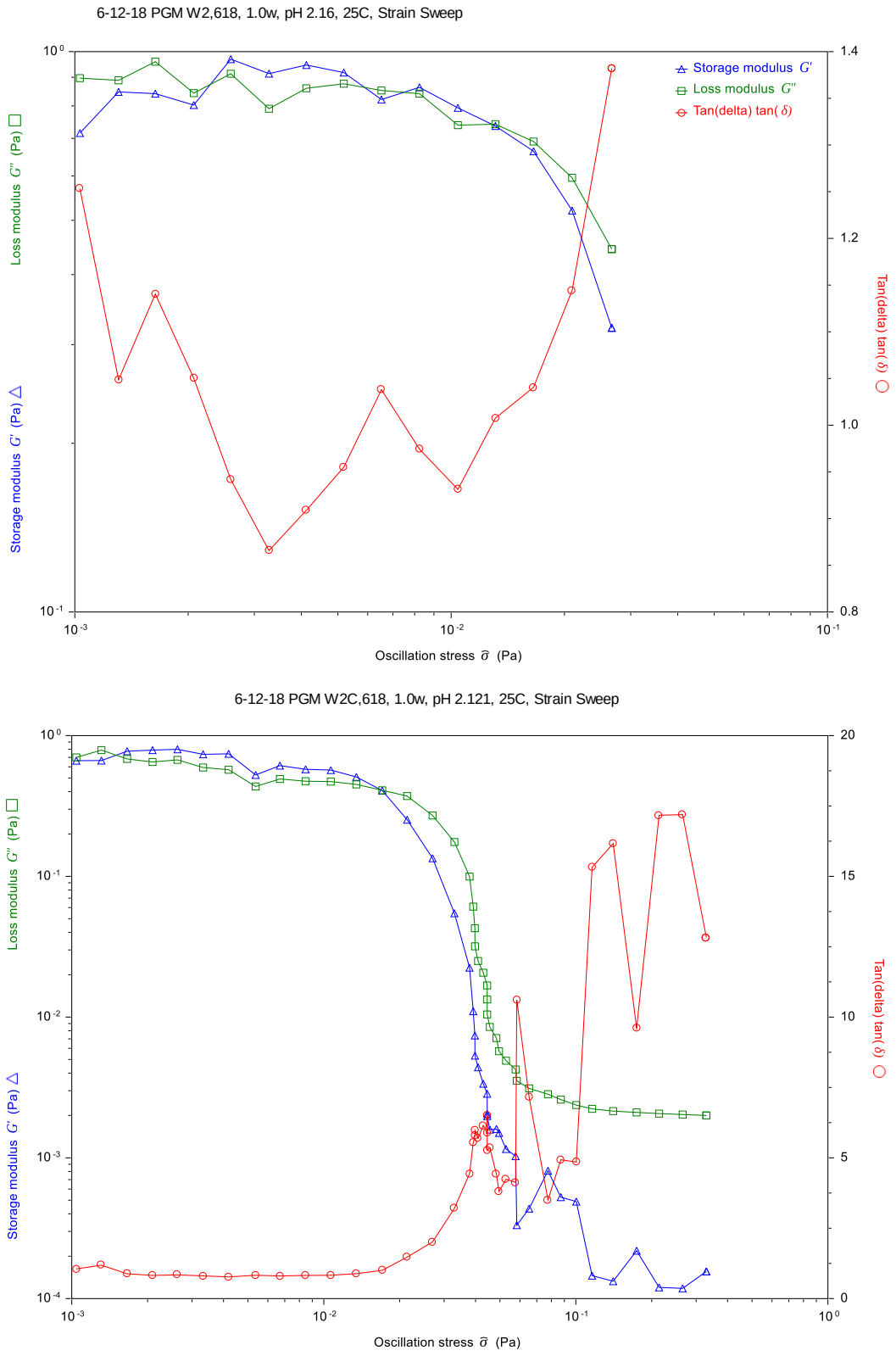

Figure 37. Stress sweeps of 10 mg/mL PGM solutions at pH 2.1 without and with 0.01 M $CaCl_2$ used to find LVR demonstrate shear thinning behavior.

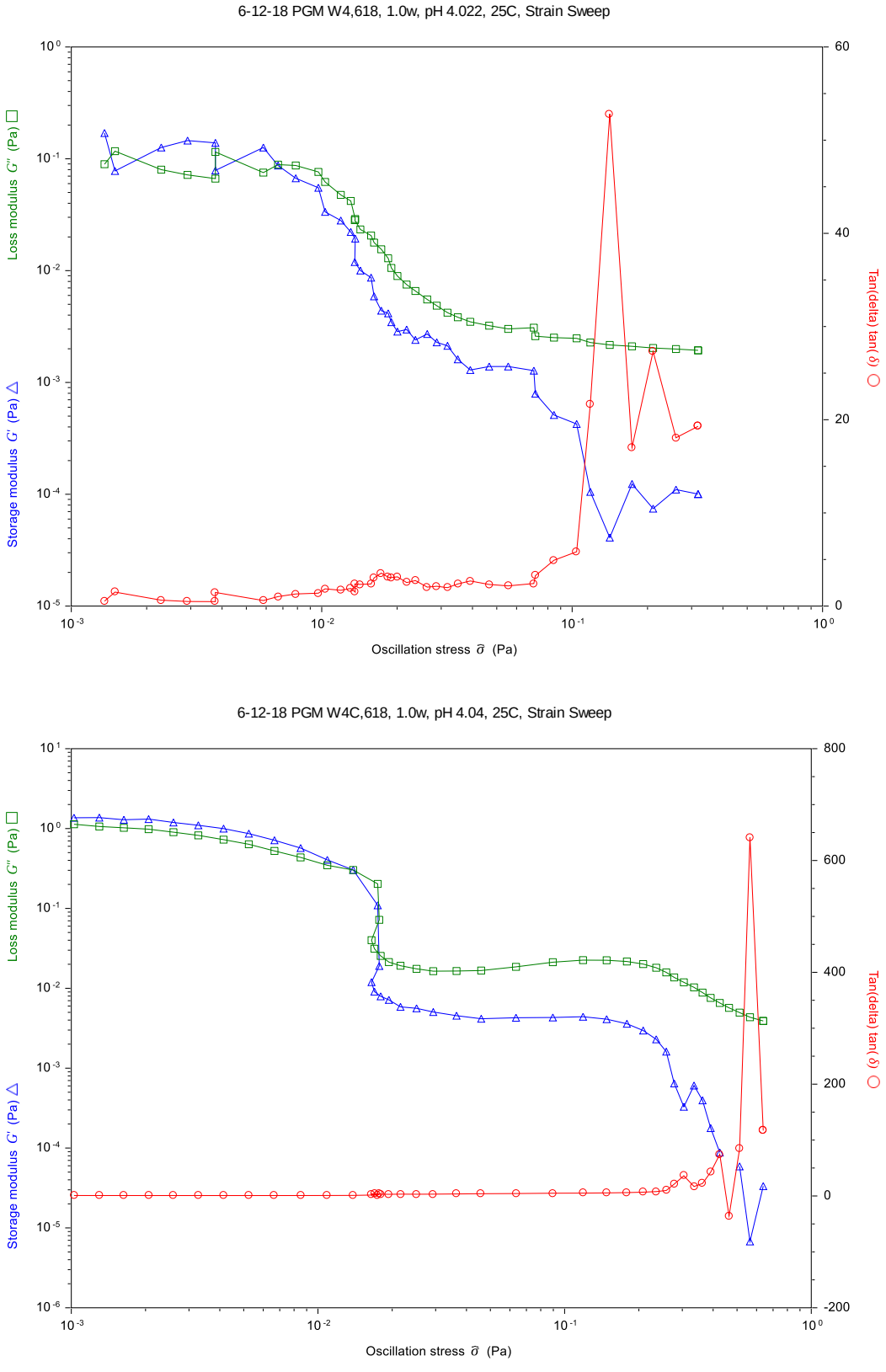

Figure 38. Stress sweeps of 10 mg/mL PGM solutions at pH 4.0 without and with 0.01 M $CaCl_2$ used to find LVR demonstrate shear thinning behavior.

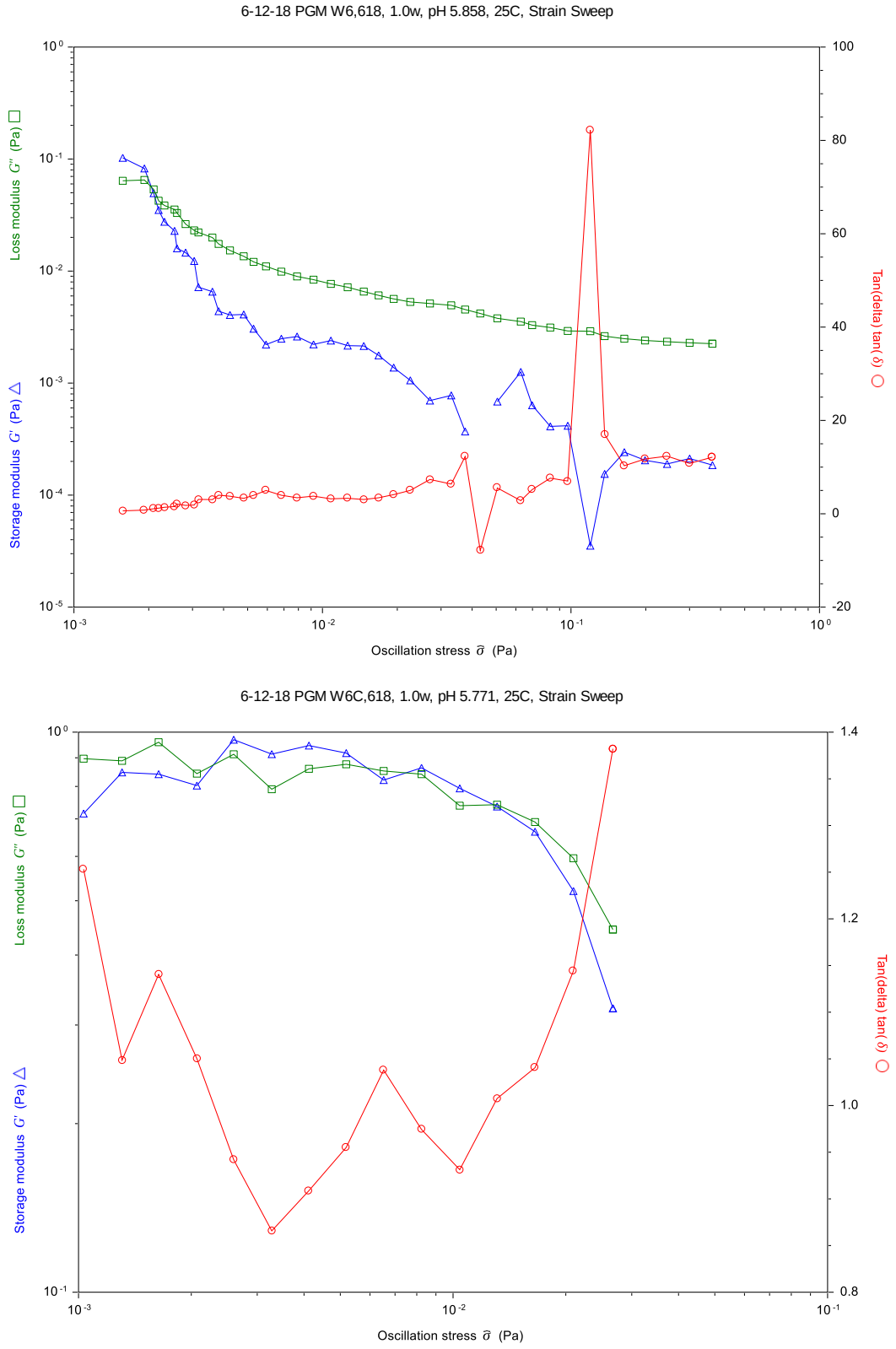

Figure 39. Stress sweeps of 10 mg/mL PGM solutions at pH 5.8 without and with 0.01 M $CaCl_2$ used to find LVR demonstrate shear thinning behavior.

C2. Effect of Mucin Concentration on Rheological Properties

Higher concentrations of PGM (20-60 mg/mL) were shown to increase viscoelastic properties, but this was not examined in depth as it is not a surprising or very interesting finding. The figure below demonstrates this finding, which is a result of increased PGM particle interactions due to increased concentration in solution.

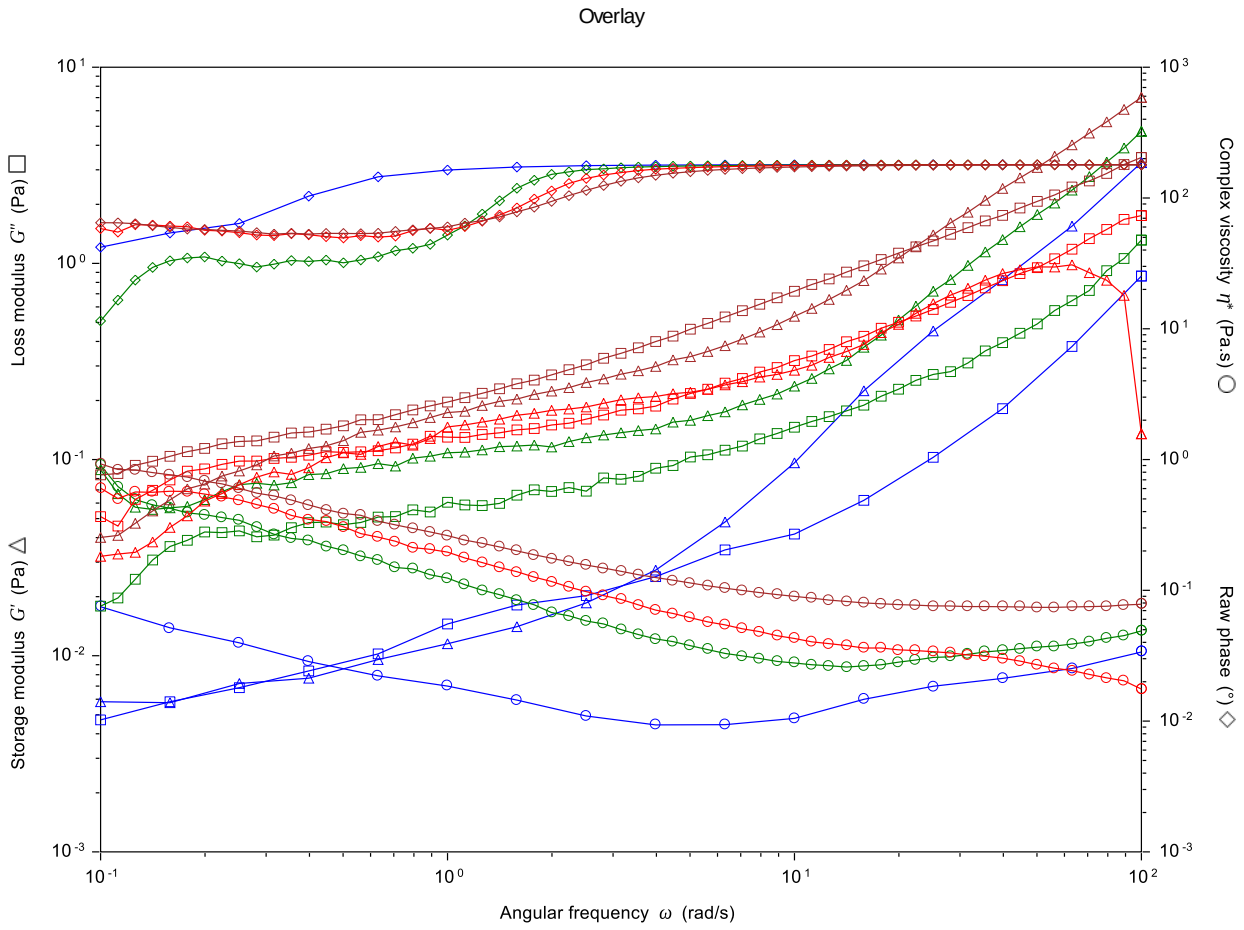

Figure 40. PGM solutions at 10 mg/mL (blue) shown to have approximately 10x lower viscoelastic properties than solutions at 20 (green), 40 (red) and 60 (brown) mg/mL.

C3. Effect of Temperature on Rheological Properties

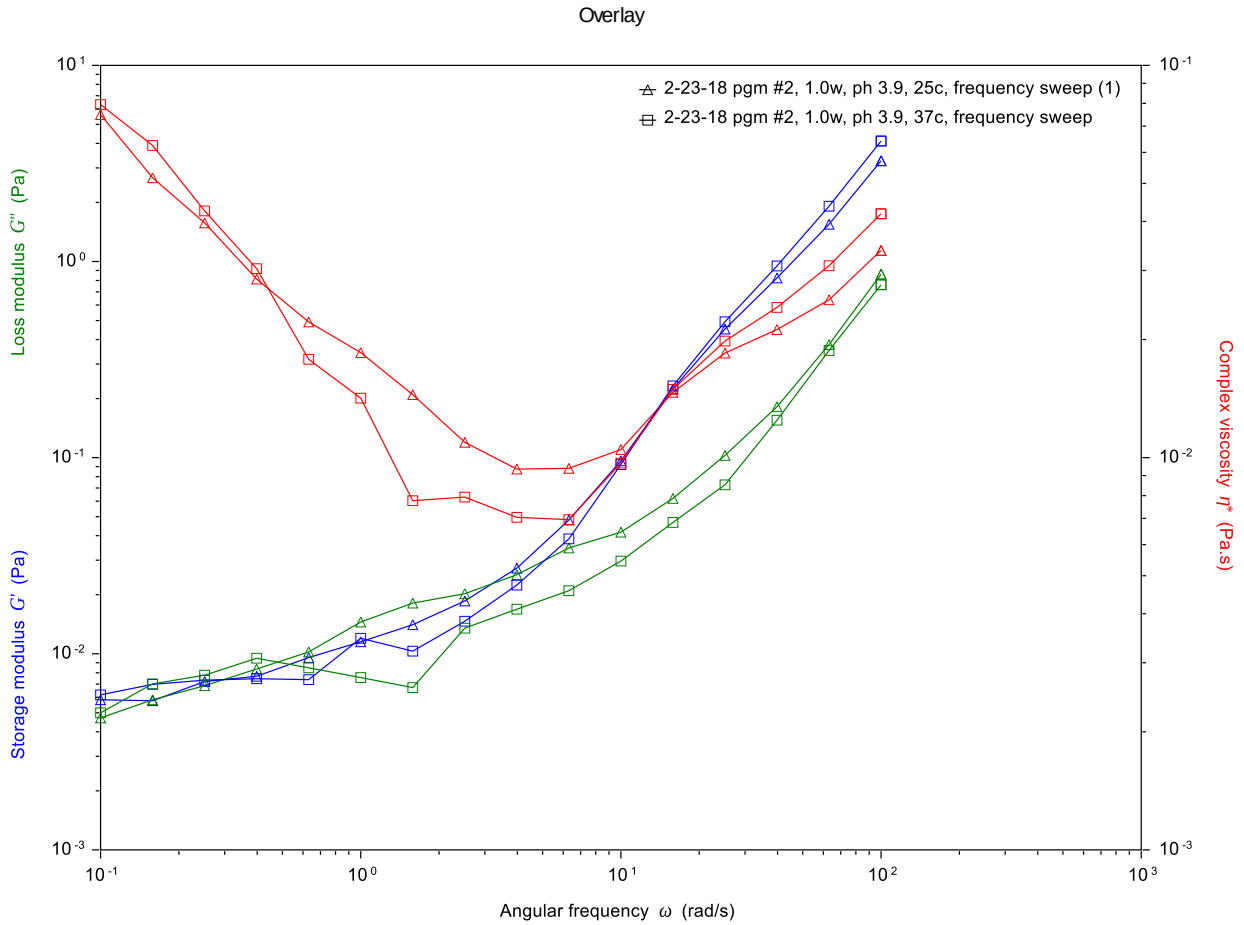

Figure 41. Sample of temperature experiment performed on a sample at pH 3.9 shows little to temperature dependence for mucin viscoelastic properties.

C4. Flat Plate Surface Tension Experiments

Surface tension experiments were performed using a Wilhelmy (flat) plate at first, but this proved to be an issue, as the surface tension values continued decreasing after the plate was initially lowered into the solution. This was not investigated thoroughly and the Du Noüy ring method was used instead. This may demonstrate a local shear-thinning response to the insertion of the plate or may be a result of local electrostatic effects in the are immediately surrounding the plate.

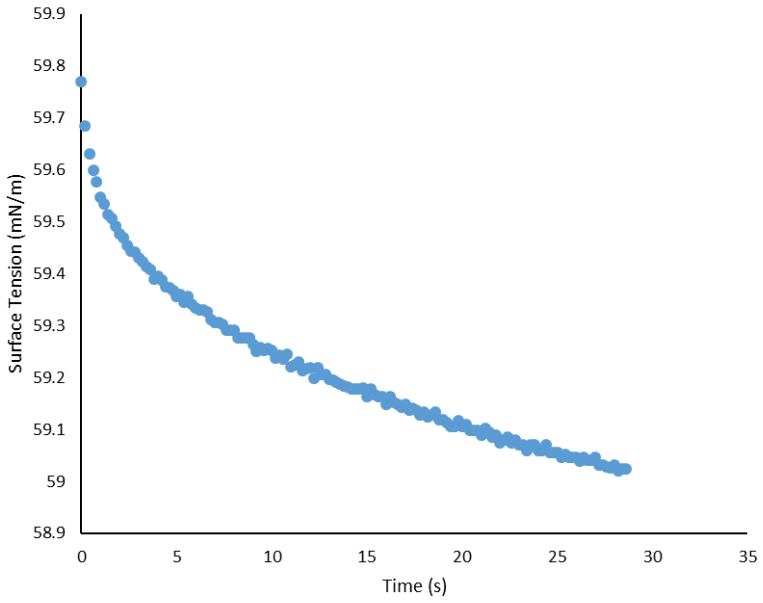

Figure 42. Surface tension measurement of a 10 mg/mL PGM solution at pH 2 with 0.01 M added $CaCl_2$.

C5. Refractive Index of Small Molecule-Doped Samples

Table 5. Refractive index of aqueous PGM samples at various concentrations of PGM and ChCL.

ChCl Sample	10 mg/mL PGM		1 mg/mL PGM		0.1 mg/mL PGM	
C1	ChCl conc. (mg/mL)	average	ChCl conc. (mg/mL)	average	ChCl conc. (mg/mL)	average
	1.40E-03	1.3341	1.40E-04	1.3327	1.40E-05	1.3325
C2	ChCl conc. (mg/mL)	average	ChCl conc. (mg/mL)	average	ChCl conc. (mg/mL)	average
	1.40E-02	1.3340	1.40E-03	1.3327	1.40E-04	1.3325
C4	ChCl conc. (mg/mL)	average	ChCl conc. (mg/mL)	average	ChCl conc. (mg/mL)	average
	1.40E-01	1.3341	1.40E-02	1.3327	1.40E-03	1.3325
C6	ChCl conc. (mg/mL)	average	ChCl conc. (mg/mL)	average	ChCl conc. (mg/mL)	average
	1.40	1.3342	0.14	1.3327	0.01	1.3325

ChCl Sample	10 mg/mL PGM		1 mg/mL PGM		0.1 mg/mL PGM	
C7	ChCl conc. (mg/mL)	average	ChCl conc. (mg/mL)	average	ChCl conc. (mg/mL)	average
	13.96	1.3360	1.40	1.3329	0.14	1.3325

Table 6. Refractive index of aqueous PGM samples at various concentrations of PGM and PBA.

PBA Sample	10 mg/mL PGM		1 mg/mL PGM		0.1 mg/mL PGM	
P1	PBA conc. (mg/mL)	average	PBA conc. (mg/mL)	average	PBA conc. (mg/mL)	average
	1.22E-03	1.3340	1.22E-04	1.3327	1.22E-05	1.3325
P2	PBA conc. (mg/mL)	average	PBA conc. (mg/mL)	average	PBA conc. (mg/mL)	average
	1.22E-02	1.3340	1.22E-03	1.3327	1.22E-04	1.3326
P4	PBA conc. (mg/mL)	average	PBA conc. (mg/mL)	average	PBA conc. (mg/mL)	average
	1.22E-01	1.3340	1.22E-02	1.3327	1.22E-03	1.3325
P6	PBA conc. (mg/mL)	average	PBA conc. (mg/mL)	average	PBA conc. (mg/mL)	average
	1.22	1.3342	0.12	1.3327	0.01	1.3325
P7	PBA conc. (mg/mL)	average	PBA conc. (mg/mL)	average	PBA conc. (mg/mL)	average
	12.19	1.3365	1.22	1.3329	0.12	1.3325

Table 7. Refractive index of aqueous PGM samples at various concentrations of PGM and TEA.

Sample	10 mg/mL PGM		1 mg/mL PGM		0.1 mg/mL PGM	
T1	TEA conc. (mg/mL)	average	TEA conc. (mg/mL)	average	TEA conc. (mg/mL)	average

Sample	10 mg/mL PGM		1 mg/mL PGM		0.1 mg/mL PGM	
	1.49E-03	1.3340	1.49E-04	1.3327	1.49E-05	1.3325
T2	TEA conc. (mg/mL)	average	TEA conc. (mg/mL)	average	TEA conc. (mg/mL)	average
	1.49E-02	1.3339	1.49E-03	1.3326	1.49E-04	1.3324
T4	TEA conc. (mg/mL)	average	TEA conc. (mg/mL)	average	TEA conc. (mg/mL)	average
	1.49E-01	1.3340	1.49E-02	1.3326	1.49E-03	1.3324
T6	TEA conc. (mg/mL)	average	TEA conc. (mg/mL)	average	TEA conc. (mg/mL)	average
	1.49	1.3343	0.15	1.3326	0.01	1.3324
T7	TEA conc. (mg/mL)	average	TEA conc. (mg/mL)	average	TEA conc. (mg/mL)	average
	14.92	1.3362	1.49	1.3328	0.15	1.3325

References

(1) Bansil, R.; Turner, B. S. The Biology of Mucus: Composition, Synthesis and Organization. *Advanced Drug Delivery Reviews* **2018**, *124*, 3–15. https://doi.org/10.1016/j.addr.2017.09.023.

(2) Facultad Medicina Buap. Rinosinusitis Aguda, 19:35:04 UTC.

(3) Mucus in Invertebrates https://www.nature.com/articles/200946b0 (accessed Aug 16, 2019). https://doi.org/10.1038/200946b0.

(4) Gugler, E.; Pallavicini, C. J.; Swerdlow, H.; di Sant'Agnese, P. A. The Role of Calcium in Submaxillary Saliva of Patients with Cystic Fibrosis. *The Journal of Pediatrics* **1967**, *71* (4), 585–588. https://doi.org/10.1016/S0022-3476(67)80114-8.

(5) Forstner, J. F.; Forstner, G. G. Effects of Calcium on Intestinal Mucin: Implications for Cystic Fibrosis. *Pediatric Research* **1976**, *10* (6), 609–613. https://doi.org/10.1203/00006450-197606000-00009.

(6) Ridley, C.; Thornton, D. J. Mucins: The Frontline Defence of the Lung. *Biochemical Society Transactions* **2018**, BST20170402. https://doi.org/10.1042/BST20170402.

(7) Ridley, C.; Kouvatsos, N.; Raynal, B. D.; Howard, M.; Collins, R. F.; Desseyn, J.-L.; Jowitt, T. A.; Baldock, C.; Davis, C. W.; Hardingham, T. E.; et al. Assembly of the Respiratory Mucin MUC5B A NEW MODEL FOR A GEL-FORMING MUCIN. *J. Biol. Chem.* **2014**, *289* (23), 16409–16420. https://doi.org/10.1074/jbc.M114.566679.

(8) Wickström, C.; Davies, J. R.; Eriksen, G. V.; Veerman, E. C.; Carlstedt, I. MUC5B Is a Major Gel-Forming, Oligomeric Mucin from Human Salivary Gland, Respiratory Tract and Endocervix: Identification of Glycoforms and C-Terminal Cleavage. *Biochem. J.* **1998**, *334 (Pt 3)*, 685–693. https://doi.org/10.1042/bj3340685.

(9) Bansil, R.; Turner, B. S. Mucin Structure, Aggregation, Physiological Functions and Biomedical Applications. *Current Opinion in Colloid & Interface Science* **2006**, *11* (2), 164–170. https://doi.org/10.1016/j.cocis.2005.11.001.

(10) Lai, S. K.; Wang, Y.-Y.; Wirtz, D.; Hanes, J. Micro- and Macrorheology of Mucus. *Advanced Drug Delivery Reviews* **2009**, *61* (2), 86–100. https://doi.org/10.1016/j.addr.2008.09.012.

(11) Cone, R. A. Barrier Properties of Mucus. *Advanced Drug Delivery Reviews* **2009**, *61* (2), 75–85. https://doi.org/10.1016/j.addr.2008.09.008.

(12) Svensson, O.; Thuresson, K.; Arnebrant, T. Interactions between Drug Delivery Particles and Mucin in Solution and at Interfaces. *Langmuir* **2008**, *24* (6), 2573–2579. https://doi.org/10.1021/la702680x.

(13) Shen, J.; Wang, Y.; Ping, Q.; Xiao, Y.; Huang, X. Mucoadhesive Effect of Thiolated PEG Stearate and Its Modified NLC for Ocular Drug Delivery. *Journal of Controlled Release* **2009**, *137* (3), 217–223. https://doi.org/10.1016/j.jconrel.2009.04.021.

(14) Chen, E. Y.; Daley, D.; Wang, Y.-C.; Garnica, M.; Chen, C.-S.; Chin, W.-C. Functionalized Carboxyl Nanoparticles Enhance Mucus Dispersion and Hydration. *Scientific Reports* **2012**, *2*, 211. https://doi.org/10.1038/srep00211.

(15) Khutoryanskiy, V. V. Advances in Mucoadhesion and Mucoadhesive Polymers. *Macromolecular Bioscience* **2011**, *11* (6), 748–764. https://doi.org/10.1002/mabi.201000388.

(16) Liu, S.; Jones, L.; Gu, F. X. Development of Mucoadhesive Drug Delivery System Using Phenylboronic Acid Functionalized Poly(D,L-Lactide)-b-Dextran Nanoparticles. *Macromolecular Bioscience* **2012**, *12* (12), 1622–1626. https://doi.org/10.1002/mabi.201200216.

(17) Zhang, X.; Chen, G.; Zhang, T.; Ma, Z.; Wu, B. Effects of PEGylated lipid nanoparticles on the oral absorption of one BCS II drug: a mechanistic investigation https://www.dovepress.com/effects-of-pegylated-lipid-nanoparticles-on-the-oral-absorption-of-one-peer-reviewed-article-IJN (accessed Jul 13, 2018). https://doi.org/10.2147/IJN.S73340.

(18) Shitrit, Y.; Bianco-Peled, H. Acrylated Chitosan for Mucoadhesive Drug Delivery Systems. *International Journal of Pharmaceutics* **2017**, *517* (1), 247–255. https://doi.org/10.1016/j.ijpharm.2016.12.023.

(19) Ho, D.-K.; Frisch, S.; Biehl, A.; Terriac, E.; De Rossi, C.; Schwarzkopf, K.; Lautenschläger, F.; Loretz, B.; Murgia, X.; Lehr, C.-M. Farnesylated Glycol Chitosan as a Platform for Drug Delivery: Synthesis, Characterization, and Investigation of Mucus–Particle Interactions. *Biomacromolecules* **2018**, *19* (8), 3489–3501. https://doi.org/10.1021/acs.biomac.8b00795.

(20) Dawson, M.; Krauland, E.; Wirtz, D.; Hanes, J. Transport of Polymeric Nanoparticle Gene Carriers in Gastric Mucus. *Biotechnology Progress* **2004**, *20* (3), 851–857. https://doi.org/10.1021/bp0342553.

(21) Bhattacharjee, S.; Mahon, E.; Harrison, S. M.; McGetrick, J.; Muniyappa, M.; Carrington, S. D.; Brayden, D. J. Nanoparticle Passage through Porcine Jejunal Mucus: Microfluidics and Rheology. *Nanomedicine: Nanotechnology, Biology and Medicine* **2017**, *13* (3), 863–873. https://doi.org/10.1016/j.nano.2016.11.017.

(22) Georgiades, P.; Pudney, P. D. A.; Thornton, D. J.; Waigh, T. A. Particle Tracking Microrheology of Purified Gastrointestinal Mucins. *Biopolymers* **2014**, *101* (4), 366–377. https://doi.org/10.1002/bip.22372.

(23) Abdulkarim, M.; Agulló, N.; Cattoz, B.; Griffiths, P.; Bernkop-Schnürch, A.; Borros, S. G.; Gumbleton, M. Nanoparticle Diffusion within Intestinal Mucus: Three-Dimensional Response Analysis Dissecting the Impact of Particle Surface Charge, Size and

Heterogeneity across Polyelectrolyte, Pegylated and Viral Particles. *European Journal of Pharmaceutics and Biopharmaceutics* **2015**, *97*, 230–238. https://doi.org/10.1016/j.ejpb.2015.01.023.

(24) Chen, E. Y. T.; Wang, Y.-C.; Chen, C.-S.; Chin, W.-C. Functionalized Positive Nanoparticles Reduce Mucin Swelling and Dispersion. *PLOS ONE* **2010**, *5* (11), e15434. https://doi.org/10.1371/journal.pone.0015434.

(25) Perez-Vilar, J.; Boucher, R. C. Reevaluating Gel-Forming Mucins' Roles in Cystic Fibrosis Lung Disease. *Free Radical Biology and Medicine* **2004**, *37* (10), 1564–1577. https://doi.org/10.1016/j.freeradbiomed.2004.07.027.

(26) Henderson, A. G.; Ehre, C.; Button, B.; Abdullah, L. H.; Cai, L.-H.; Leigh, M. W.; DeMaria, G. C.; Matsui, H.; Donaldson, S. H.; Davis, C. W.; et al. Cystic Fibrosis Airway Secretions Exhibit Mucin Hyperconcentration and Increased Osmotic Pressure. *J Clin Invest* **2014**, *124* (7), 3047–3060. https://doi.org/10.1172/JCI73469.

(27) Tang, X. X.; Ostedgaard, L. S.; Hoegger, M. J.; Moninger, T. O.; Karp, P. H.; McMenimen, J. D.; Choudhury, B.; Varki, A.; Stoltz, D. A.; Welsh, M. J. Acidic PH Increases Airway Surface Liquid Viscosity in Cystic Fibrosis. *J Clin Invest* **2016**, *126* (3), 879–891. https://doi.org/10.1172/JCI83922.

(28) Bansil, R.; Celli, J.; Hardcastle, J.; Turner, B. The Influence of Mucus Microstructure and Rheology in Helicobacter Pylori Infection. *Front. Immunol.* **2013**, *4*. https://doi.org/10.3389/fimmu.2013.00310.

(29) Cao, X.; Bansil, R.; Bhaskar, K. R.; Turner, B. S.; LaMont, J. T.; Niu, N.; Afdhal, N. H. PH-Dependent Conformational Change of Gastric Mucin Leads to Sol-Gel Transition. *Biophysical Journal* **1999**, *76* (3), 1250–1258. https://doi.org/10.1016/S0006-3495(99)77288-7.

(30) Lafitte, G.; Söderman, O.; Thuresson, K.; Davies, J. PFG-NMR Diffusometry: A Tool for Investigating the Structure and Dynamics of Noncommercial Purified Pig Gastric Mucin in a Wide Range of Concentrations. *Biopolymers 86* (2), 165–175. https://doi.org/10.1002/bip.20717.

(31) Bhaskar, K. R.; Gong, D. H.; Bansil, R.; Pajevic, S.; Hamilton, J. A.; Turner, B. S.; LaMont, J. T. Profound Increase in Viscosity and Aggregation of Pig Gastric Mucin at Low PH. *American Journal of Physiology-Gastrointestinal and Liver Physiology* **1991**, *261* (5), G827–G832. https://doi.org/10.1152/ajpgi.1991.261.5.G827.

(32) Pettersson, T.; Feldötö, Z.; Claesson, P. M.; Dedinaite, A. The Effect of Salt Concentration and Cation Valency on Interactions Between Mucin-CoatedHydrophobic Surfaces. In *Surface and Interfacial Forces – From Fundamentals to Applications*; Auernhammer, G. K., Butt, H.-J., Vollmer, D., Eds.; Progress in Colloid and Polymer Science; Springer Berlin Heidelberg, 2008; pp 1–10.

(33) Bell, A. E.; Sellers, L. A.; Allen, A.; Cunliffe, W. J.; Morris, E. R.; Ross-Murphy, S. B. Properties of Gastric and Duodenal Mucus: Effect of Proteolysis, Disulfide Reduction,

Bile, Acid, Ethanol, and Hypertonicity on Mucus Gel Structure. *Gastroenterology* **1985**, *88* (1, Part 2), 269–280. https://doi.org/10.1016/S0016-5085(85)80180-3.

(34) Bromberg, L. E.; Barr, D. P. Self-Association of Mucin. *Biomacromolecules* **2000**, *1* (3), 325–334. https://doi.org/10.1021/bm005532m.

(35) Meldrum, O. W.; Yakubov, G. E.; Bonilla, M. R.; Deshmukh, O.; McGuckin, M. A.; Gidley, M. J. Mucin Gel Assembly Is Controlled by a Collective Action of Non-Mucin Proteins, Disulfide Bridges, Ca 2+ -Mediated Links, and Hydrogen Bonding. *Scientific Reports* **2018**, *8* (1), 5802. https://doi.org/10.1038/s41598-018-24223-3.

(36) Celli, J. P.; Turner, B. S.; Afdhal, N. H.; Ewoldt, R. H.; McKinley, G. H.; Bansil, R.; Erramilli, S. Rheology of Gastric Mucin Exhibits a PH-Dependent Sol−Gel Transition. *Biomacromolecules* **2007**, *8* (5), 1580–1586. https://doi.org/10.1021/bm0609691.

(37) Hong, Z.; Chasan, B.; Bansil, R.; Turner, B. S.; Bhaskar, K. R.; Afdhal, N. H. Atomic Force Microscopy Reveals Aggregation of Gastric Mucin at Low PH. *Biomacromolecules* **2005**, *6* (6), 3458–3466. https://doi.org/10.1021/bm0505843.

(38) Bansil, R.; Stanley, E.; LaMont, J. T. Mucin Biophysics. *Annu. Rev. Physiol.* **1995**, *57*, 635–657. https://doi.org/10.1146/annurev.ph.57.030195.003223.

(39) Veerman, E. C.; Valentijn-Benz, M.; Nieuw Amerongen, A. V. Viscosity of Human Salivary Mucins: Effect of PH and Ionic Strength and Role of Sialic Acid. *J Biol Buccale* **1989**, *17* (4), 297–306.

(40) Espinosa, M.; Noé, G.; Troncoso, C.; Ho, S. B.; Villalón, M. Acidic PH and Increasing [Ca2+] Reduce the Swelling of Mucins in Primary Cultures of Human Cervical Cells. *Hum Reprod* **2002**, *17* (8), 1964–1972. https://doi.org/10.1093/humrep/17.8.1964.

(41) Lai, S. K.; Wang, Y.-Y.; Hanes, J. Mucus-Penetrating Nanoparticles for Drug and Gene Delivery to Mucosal Tissues. *Advanced Drug Delivery Reviews* **2009**, *61* (2), 158–171. https://doi.org/10.1016/j.addr.2008.11.002.

(42) Wang, Y.-Y.; Lai, S. K.; So, C.; Schneider, C.; Cone, R.; Hanes, J. Mucoadhesive Nanoparticles May Disrupt the Protective Human Mucus Barrier by Altering Its Microstructure. *PLOS ONE* **2011**, *6* (6), e21547. https://doi.org/10.1371/journal.pone.0021547.

(43) Lieleg, O.; Vladescu, I.; Ribbeck, K. Characterization of Particle Translocation through Mucin Hydrogels. *Biophysical Journal* **2010**, *98* (9), 1782–1789. https://doi.org/10.1016/j.bpj.2010.01.012.

(44) Svensson, Olof. Interactions of Mucins with Biopolymers and Drug Delivery Particles, Malmo University, 2008.

(45) McGill, S. L.; Smyth, H. D. C. Disruption of the Mucus Barrier by Topically Applied Exogenous Particles. *Mol. Pharmaceutics* **2010**, *7* (6), 2280–2288. https://doi.org/10.1021/mp100242r.

(46) Nordgård, C. T.; Nonstad, U.; Olderøy, M. Ø.; Espevik, T.; Draget, K. I. Alterations in Mucus Barrier Function and Matrix Structure Induced by Guluronate Oligomers. *Biomacromolecules* **2014**, *15* (6), 2294–2300. https://doi.org/10.1021/bm500464b.

(47) Bansil, R.; Turner, B. S. The Biology of Mucus: Composition, Synthesis and Organization. *Advanced Drug Delivery Reviews* **2018**, *124*, 3–15. https://doi.org/10.1016/j.addr.2017.09.023.

(48) Maleki, A.; Lafitte, G.; Kjøniksen, A.-L.; Thuresson, K.; Nyström, B. Effect of PH on the Association Behavior in Aqueous Solutions of Pig Gastric Mucin. *Carbohydrate Research* **2008**, *343* (2), 328–340. https://doi.org/10.1016/j.carres.2007.10.005.

(49) Tamburic, S.; Craig, D. Q. M. A Comparison of Different in Vitro Methods for Measuring Mucoadhesive Performance. *European Journal of Pharmaceutics and Biopharmaceutics* **1997**, *44* (2), 159–167. https://doi.org/10.1016/S0939-6411(97)00073-8.

(50) Wang, S.-H.; Lee, C.-W.; Chiou, A.; Wei, P.-K. Size-Dependent Endocytosis of Gold Nanoparticles Studied by Three-Dimensional Mapping of Plasmonic Scattering Images. *Journal of Nanobiotechnology* **2010**, *8*, 33. https://doi.org/10.1186/1477-3155-8-33.

(51) Jiang, Y.; Huo, S.; Mizuhara, T.; Das, R.; Lee, Y.-W.; Hou, S.; Moyano, D. F.; Duncan, B.; Liang, X.-J.; Rotello, V. M. The Interplay of Size and Surface Functionality on the Cellular Uptake of Sub-10 Nm Gold Nanoparticles. *ACS Nano* **2015**, *9* (10), 9986–9993. https://doi.org/10.1021/acsnano.5b03521.

(52) Barbero, N.; Coletti, M.; Catalano, F.; Visentin, S. Exploring Gold Nanoparticles Interaction with Mucins: A Spectroscopic-Based Study. *International Journal of Pharmaceutics* **2018**, *535* (1), 438–443. https://doi.org/10.1016/j.ijpharm.2017.11.026.

(53) Ibrahim, H. K.; El-Leithy, I. S.; Makky, A. A. Mucoadhesive Nanoparticles as Carrier Systems for Prolonged Ocular Delivery of Gatifloxacin/Prednisolone Bitherapy. *Mol. Pharmaceutics* **2010**, *7* (2), 576–585. https://doi.org/10.1021/mp900279c.

(54) Wilcox, M. D.; Van Rooij, L. K.; Chater, P. I.; Pereira de Sousa, I.; Pearson, J. P. The Effect of Nanoparticle Permeation on the Bulk Rheological Properties of Mucus from the Small Intestine. *European Journal of Pharmaceutics and Biopharmaceutics* **2015**, *96*, 484–487. https://doi.org/10.1016/j.ejpb.2015.02.029.

(55) Waigh, T. A.; Papagiannopoulos, A. Biological and Biomimetic Comb Polyelectrolytes. *Polymers* **2010**, *2* (2), 57–70. https://doi.org/10.3390/polym2020057.

(56) Crater, J. S.; Carrier, R. L. Barrier Properties of Gastrointestinal Mucus to Nanoparticle Transport. *Macromolecular Bioscience* **2010**, *10* (12), 1473–1483. https://doi.org/10.1002/mabi.201000137.

(57) Sellers, L. A.; Allen, A.; Morris, E. R.; Ross-Murphy, S. B. The Rheology of Pig Small Intestinal and Colonic Mucus: Weakening of Gel Structure by Non-Mucin Components. *Biochimica et Biophysica Acta (BBA) - General Subjects* **1991**, *1115* (2), 174–179. https://doi.org/10.1016/0304-4165(91)90027-E.

(58) Silva, C. A.; Nobre, T. M.; Pavinatto, F. J.; Oliveira, O. N. Interaction of Chitosan and Mucin in a Biomembrane Model Environment. *Journal of Colloid and Interface Science* **2012**, *376* (1), 289–295. https://doi.org/10.1016/j.jcis.2012.03.027.

(59) Madsen, J. B.; Sotres, J.; Pakkanen, K. I.; Efler, P.; Svensson, B.; Abou Hachem, M.; Arnebrant, T.; Lee, S. Structural and Mechanical Properties of Thin Films of Bovine Submaxillary Mucin versus Porcine Gastric Mucin on a Hydrophobic Surface in Aqueous Solutions. *Langmuir* **2016**, *32* (38), 9687–9696. https://doi.org/10.1021/acs.langmuir.6b02057.

(60) Lewis, A. T.; Jones, K.; Lewis, K. E.; Jones, S.; Lewis, P. D. Detection of Lewis Antigen Structural Change by FTIR Spectroscopy. *Carbohydrate Polymers* **2013**, *92* (2), 1294–1301. https://doi.org/10.1016/j.carbpol.2012.09.078.

(61) Khajehpour, M.; Dashnau, J. L.; Vanderkooi, J. M. Infrared Spectroscopy Used to Evaluate Glycosylation of Proteins. *Analytical Biochemistry* **2005**, *348* (1), 40–48.

(62) *Rheology of Complex Fluids*; Deshpande, A. P., Murali, K. J., Sunil, K. P. B., Eds.; Springer: New York, 2010.

(63) Moreira, H. R.; Munarin, F.; Gentilini, R.; Visai, L.; Granja, P. L.; Tanzi, M. C.; Petrini, P. Injectable Pectin Hydrogels Produced by Internal Gelation: PH Dependence of Gelling and Rheological Properties. *Carbohydrate Polymers* **2014**, *103*, 339–347. https://doi.org/10.1016/j.carbpol.2013.12.057.

(64) Li, L. D.; Crouzier, T.; Sarkar, A.; Dunphy, L.; Han, J.; Ribbeck, K. Spatial Configuration and Composition of Charge Modulates Transport into a Mucin Hydrogel Barrier. *Biophysical Journal* **2013**, *105* (6), 1357–1365. https://doi.org/10.1016/j.bpj.2013.07.050.

(65) Green, A. S. Modelling of Peak-Flow Wall Shear Stress in Major Airways of the Lung. *Journal of Biomechanics* **2004**, *37* (5), 661–667. https://doi.org/10.1016/j.jbiomech.2003.09.024.

(66) Kou, G.; Li, X.; Wang, Y.; Lin, M.; Zeng, Y.; Yang, X.; Yang, Y.; Gan, Z. CFD Simulation of Airflow Dynamics During Cough Based on CT-Scanned Respiratory Airway Geometries. *Symmetry* **2018**, *10* (11), 595. https://doi.org/10.3390/sym10110595.

(67) Verdugo, P.; Deyrup-Olsen, I.; Aitken, M.; Villalon, M.; Johnson, D. Molecular Mechanism of Mucin Secretion: I. The Role of Intragranular Charge Shielding. *J Dent Res* **1987**, *66* (2), 506–508. https://doi.org/10.1177/00220345870660022001.

(68) Verdugo, P. Supramolecular Dynamics of Mucus. *Cold Spring Harb Perspect Med* **2012**, *2* (11), a009597. https://doi.org/10.1101/cshperspect.a009597.

(69) Raynal, B. D. E.; Hardingham, T. E.; Sheehan, J. K.; Thornton, D. J. Calcium-Dependent Protein Interactions in MUC5B Provide Reversible Cross-Links in Salivary Mucus. *J. Biol. Chem.* **2003**, *278* (31), 28703–28710. https://doi.org/10.1074/jbc.M304632200.

(70) Lee, S.; Müller, M.; Rezwan, K.; Spencer, N. D. Porcine Gastric Mucin (PGM) at the Water/Poly(Dimethylsiloxane) (PDMS) Interface: Influence of PH and Ionic Strength on

Its Conformation, Adsorption, and Aqueous Lubrication Properties. *Langmuir* **2005**, *21* (18), 8344–8353. https://doi.org/10.1021/la050779w.

(71) Lamont, J. T. Mucus: The Front Line of Intestinal Mucosal Defense. *Annals of the New York Academy of Sciences* **1992**, *664* (1 Neuro-immuno-), 190–201. https://doi.org/10.1111/j.1749-6632.1992.tb39760.x.

(72) Tetenbaum, J.; Miller, L. M. A New Spectroscopic Approach to Examining the Role of Disulfide Bonds in the Structure and Unfolding of Soybean Trypsin Inhibitor. *Biochemistry* **2001**, *40* (40), 12215–12219. https://doi.org/10.1021/bi010796u.

(73) Caicedo, J.; Perilla, J. E. Effect of PH on the Rheological Response of Reconstituted Gastric Mucin. *Ingeniería e Investigación* **2015**, *35* (2), 43–48. https://doi.org/10.15446/ing.investig.v35n2.50019.

(74) Chuah, L. H.; Billa, N.; Roberts, C. J.; Burley, J. C.; Manickam, S. Curcumin-Containing Chitosan Nanoparticles as a Potential Mucoadhesive Delivery System to the Colon. *Pharm Dev Technol* **2013**, *18* (3), 591–599. https://doi.org/10.3109/10837450.2011.640688.

(75) Zhang, Y.; Yang, Z.; Hu, X.; Zhang, L.; Li, F.; Li, M.; Tang, X.; Xiao, W. Development and Evaluation of Mucoadhesive Nanoparticles Based on Thiolated Eudragit for Oral Delivery of Protein Drugs. *J Nanopart Res* **2015**, *17* (2), 98. https://doi.org/10.1007/s11051-015-2909-5.

(76) Zhang, Y.; Lin, X.; Du, X.; Geng, S.; Li, H.; Sun, H.; Tang, X.; Xiao, W. PH-Sensitive Thiolated Nanoparticles Facilitate the Oral Delivery of Insulin in Vitro and in Vivo. *J Nanopart Res* **2015**, *17* (2), 103. https://doi.org/10.1007/s11051-014-2847-7.

(77) Bhat, P. G.; Flanagan, D. R.; Donovan, M. D. Drug Binding to Gastric Mucus Glycoproteins. *International Journal of Pharmaceutics* **1996**, *134* (1), 15–25. https://doi.org/10.1016/0378-5173(95)04333-0.

(78) Duffy, C. V.; David, L.; Crouzier, T. Covalently-Crosslinked Mucin Biopolymer Hydrogels for Sustained Drug Delivery. *Acta Biomaterialia* **2015**, *20*, 51–59. https://doi.org/10.1016/j.actbio.2015.03.024.

(79) Alkholief, M.; Campbell, R. B. Investigating the Role of Mucin in the Delivery of Nanoparticles to Cellular Models of Human Cancer Disease: An in Vitro Study. *Nanomedicine: Nanotechnology, Biology and Medicine* **2016**, *12* (5), 1291–1302. https://doi.org/10.1016/j.nano.2016.01.007.

(80) Andreani, T.; Souza, A. L. R. de; Kiill, C. P.; Lorenzón, E. N.; Fangueiro, J. F.; Calpena, A. C.; Chaud, M. V.; Garcia, M. L.; Gremião, M. P. D.; Silva, A. M.; et al. Preparation and Characterization of PEG-Coated Silica Nanoparticles for Oral Insulin Delivery. *International Journal of Pharmaceutics* **2014**, *473* (1), 627–635. https://doi.org/10.1016/j.ijpharm.2014.07.049.

(81) Svensson, O.; Thuresson, K.; Arnebrant, T. Interactions between Chitosan-Modified Particles and Mucin-Coated Surfaces. *Journal of Colloid and Interface Science* **2008**, *325* (2), 346–350. https://doi.org/10.1016/j.jcis.2008.06.013.

(82) Suk, J. S.; Xu, Q.; Kim, N.; Hanes, J.; Ensign, L. M. PEGylation as a Strategy for Improving Nanoparticle-Based Drug and Gene Delivery. *Advanced Drug Delivery Reviews* **2016**, *99*, 28–51. https://doi.org/10.1016/j.addr.2015.09.012.

(83) Thasneem, Y. M.; Rekha, M. R.; Sajeesh, S.; Sharma, C. P. Biomimetic Mucin Modified PLGA Nanoparticles for Enhanced Blood Compatibility. *Journal of Colloid and Interface Science* **2013**, *409*, 237–244. https://doi.org/10.1016/j.jcis.2013.07.004.

(84) Wagner, C. E.; Turner, B. S.; Rubinstein, M.; McKinley, G. H.; Ribbeck, K. A Rheological Study of the Association and Dynamics of MUC5AC Gels. *Biomacromolecules* **2017**, *18* (11), 3654–3664. https://doi.org/10.1021/acs.biomac.7b00809.

(85) Li, C.; Liu, Z.; Yan, X.; Lu, W.; Liu, Y. Mucin-Controlled Drug Release from Mucoadhesive Phenylboronic Acid-Rich Nanoparticles. *International Journal of Pharmaceutics* **2015**, *479* (1), 261–264. https://doi.org/10.1016/j.ijpharm.2014.12.011.

(86) Prosperi-Porta, G.; Kedzior, S.; Muirhead, B.; Sheardown, H. Phenylboronic-Acid-Based Polymeric Micelles for Mucoadhesive Anterior Segment Ocular Drug Delivery. *Biomacromolecules* **2016**, *17* (4), 1449–1457. https://doi.org/10.1021/acs.biomac.6b00054.

(87) Yan, J.; Springsteen, G.; Deeter, S.; Wang, B. The Relationship among PKa, PH, and Binding Constants in the Interactions between Boronic Acids and Diols—It Is Not as Simple as It Appears. *Tetrahedron* **2004**, *60* (49), 11205–11209. https://doi.org/10.1016/j.tet.2004.08.051.

(88) Fiume, M. M.; Heldreth, B.; Bergfeld, W. F.; Belsito, D. V.; Hill, R. A.; Klaassen, C. D.; Liebler, D.; Marks, J. G.; Shank, R. C.; Slaga, T. J.; et al. Safety Assessment of Triethanolamine and Triethanolamine-Containing Ingredients as Used in Cosmetics. *Int. J. Toxicol.* **2013**, *32* (3 Suppl), 59S-83S. https://doi.org/10.1177/1091581813488804.

(89) PubChem. Choline chloride https://pubchem.ncbi.nlm.nih.gov/compound/6209 (accessed Aug 16, 2019).

(90) PubChem. Phenylboronic acid https://pubchem.ncbi.nlm.nih.gov/compound/66827 (accessed Aug 16, 2019).

(91) PubChem. Triethanolamine https://pubchem.ncbi.nlm.nih.gov/compound/7618 (accessed Aug 16, 2019).

(92) CHOLINE CHLORIDE | CAMEO Chemicals | NOAA https://cameochemicals.noaa.gov/chemical/20029 (accessed Aug 16, 2019).

(93) Trolamine https://www.drugbank.ca/drugs/DB13747 (accessed Aug 16, 2019).

(94) Phenyl Boronic Acid https://www.drugbank.ca/drugs/DB01795 (accessed Aug 16, 2019).

(95) Salgın, S.; Salgın, U.; Bahadır, S. Zeta Potentials and Isoelectric Points of Biomolecules: The Effects of Ion Types and Ionic Strengths. *Int. J. Electrochem. Sci.* **2012**, *7*, 11.

(96) Saitoh, H.; Hasegawa, N.; Kawai, S.; Miyazaki, K.; Arita, T. Interaction of Tertiary Amines and Quaternary Ammonium Compounds with Gastrointestinal Mucin. *Journal of Pharmacobio-Dynamics* **1986**, *9* (12), 1008–1014. https://doi.org/10.1248/bpb1978.9.1008.

(97) Andreani, T.; Miziara, L.; Lorenzón, E. N.; de Souza, A. L. R.; Kiill, C. P.; Fangueiro, J. F.; Garcia, M. L.; Gremião, P. D.; Silva, A. M.; Souto, E. B. Effect of Mucoadhesive Polymers on the in Vitro Performance of Insulin-Loaded Silica Nanoparticles: Interactions with Mucin and Biomembrane Models. *European Journal of Pharmaceutics and Biopharmaceutics* **2015**, *93*, 118–126. https://doi.org/10.1016/j.ejpb.2015.03.027.

(98) Ivanov, A. E.; Solodukhina, N.; Wahlgren, M.; Nilsson, L.; Vikhrov, A. A.; Nikitin, M. P.; Orlov, A. V.; Nikitin, P. I.; Kuzimenkova, M. V.; Zubov, V. P. Reversible Conformational Transitions of a Polymer Brush Containing Boronic Acid and Its Interaction with Mucin Glycoprotein. *Macromolecular Bioscience* **2011**, *11* (2), 275–284. https://doi.org/10.1002/mabi.201000295.

(99) Oh, S.; Borrós, S. Mucoadhesion vs Mucus Permeability of Thiolated Chitosan Polymers and Their Resulting Nanoparticles Using a Quartz Crystal Microbalance with Dissipation (QCM-D). *Colloids and Surfaces B: Biointerfaces* **2016**, *147*, 434–441. https://doi.org/10.1016/j.colsurfb.2016.08.030.

(100) Ivarsson, D.; Wahlgren, M. Comparison of in Vitro Methods of Measuring Mucoadhesion: Ellipsometry, Tensile Strength and Rheological Measurements. *Colloids and Surfaces B: Biointerfaces* **2012**, *92*, 353–359. https://doi.org/10.1016/j.colsurfb.2011.12.020.

(101) Sircar, S.; Keener, J. P.; Fogelson, A. L. The Effect of Divalent vs. Monovalent Ions on the Swelling of Mucin-like Polyelectrolyte Gels: Governing Equations and Equilibrium Analysis. *J Chem Phys* **2013**, *138* (1). https://doi.org/10.1063/1.4772405.

(102) Lu, S.; Tien, L. S.; Tu, Y.-C.; Pang, Y.; Fan, L. Mucus Secretion and Calcium Mobilization in Airway Submucosal Gland Cell; 2017.

(103) Stöber, W.; Fink, A.; Bohn, E. Controlled Growth of Monodisperse Silica Spheres in the Micron Size Range. *Journal of Colloid and Interface Science* **1968**, *26* (1), 62–69. https://doi.org/10.1016/0021-9797(68)90272-5.

(104) Klapiszewski, Ł.; Królak, M.; Jesionowski, T. Silica Synthesis by the Sol-Gel Method and Its Use in the Preparation of Multifunctional Biocomposites. *cent.eur.j.chem.* **2014**, *12* (2), 173–184. https://doi.org/10.2478/s11532-013-0370-9.

(105) SolGelCartoon.png (1116×1017) https://upload.wikimedia.org/wikipedia/commons/f/f0/SolGelCartoon.png (accessed Aug 15, 2019).

(106) Liu, Q.; Xu, Z.; Finch, J. A.; Egerton, R. A Novel Two-Step Silica-Coating Process for Engineering Magnetic Nanocomposites. *Chem. Mater.* **1998**, *10* (12), 3936–3940. https://doi.org/10.1021/cm980370a.

(107) Zdarta, J.; Sałek, K.; Kołodziejczak-Radzimska, A.; Siwińska-Stefańska, K.; Szwarc-Rzepka, K.; Norman, M.; Klapiszewski, Ł.; Bartczak, P.; Kaczorek, E.; Jesionowski, T. Immobilization of Amano Lipase A onto Stöber Silica Surface: Process Characterization and Kinetic Studies. *Open Chemistry* **2014**, *13* (1). https://doi.org/10.1515/chem-2015-0017.

(108) Sun, Di; Kang, Shifei; Liu, Chenglu; Lu, Qijie; Cui, Lifeng; Hu, Bing. Effect of Zeta Potential and Particle Size on the Stability of SiO2 Nanospheres as Carrier for Ultrasound Imaging Contrast Agents. *International Journal of Electrochemical Science* **2016**, 8520–8529. https://doi.org/10.20964/2016.10.30.

(109) Griffiths, P. C.; Cattoz, B.; Ibrahim, M. S.; Anuonye, J. C. Probing the Interaction of Nanoparticles with Mucin for Drug Delivery Applications Using Dynamic Light Scattering. *European Journal of Pharmaceutics and Biopharmaceutics* **2015**, *97*, 218–222. https://doi.org/10.1016/j.ejpb.2015.05.004.

(110) Lieleg, O.; Vladescu, I.; Ribbeck, K. Characterization of Particle Translocation through Mucin Hydrogels. *Biophysical Journal* **2010**, *98* (9), 1782–1789. https://doi.org/10.1016/j.bpj.2010.01.012.

(111) Meldrum, O. W.; Yakubov, G. E.; Gartaula, G.; McGuckin, M. A.; Gidley, M. J. Mucoadhesive Functionality of Cell Wall Structures from Fruits and Grains: Electrostatic and Polymer Network Interactions Mediated by Soluble Dietary Polysaccharides. *Scientific Reports* **2017**, *7* (1), 15794. https://doi.org/10.1038/s41598-017-16090-1.

(112) Nikonenko, N. A.; Bushnak, B. A.; Keddie, J. L. Spectroscopic Ellipsometry of Mucin Layers on an Amphiphilic Diblock Copolymer Surface, Spectroscopic Ellipsometry of Mucin Layers on an Amphiphilic Diblock Copolymer Surface. *Appl Spectrosc* **2009**, *63* (8), 889–898. https://doi.org/10.1366/000370209788964449.